



Deutsches Zentrum
für Luft- und Raumfahrt

University College Dublin

MSc Space Science and Technology

Internship Report: Multi-function Optical Transceiver for Satellite Communications

Danniel Osoianu

24200421

DLR Supervisor: Dr. Marcin Wojciech Ziarko

UCD Supervisor: Dr. Rebeca Garcia Lopez

August 25, 2025

1 Statement of Original Authorship

I hereby certify that the submitted work is my own work, was completed while registered as a candidate for the degree stated on the Title Page, and I have not obtained a degree elsewhere on the basis of the research presented in this submitted work.

2 Acknowledgements

I wish to thank those who have helped me through this internship. Specifically , I would like to thank my supervisor Marcin Ziarko for warmly welcoming me into the DLR KN institute, guiding me through the field of photonics and optical communications, and for always being there to help with questions, issues and tasks. I would also like to thank the other members of the EPIC team Giulio Terresanta and Nicola Bergamasco for their kind help in the lab, allowing me to learn about PICs through their work and keen interest. I also wish to thank the DLR football club for motivating me and giving me a nice distraction after sitting at the computer all day.

I want to extend my thanks to a number of faculty members in UCD for their help throughout the Masters course, specifically Lorraine Hanlon, who has orchestrated this Masters programme to be informative, ambitious and above all else, fun. I want to thank David Murphy for his lectures on spacecraft telecommunications which piqued my interest, and for providing me some papers on optical telecommunications in preparation for the interview for this internship.

Finally, I want to thank all of my friends and family who have supported me throughout this course and internship non-stop. I couldn't have done it without them.

3 Abstract

This report presents an investigation into the performance of commercial on–off keying transceivers under both direct detection and coherent reception schemes, supported by the development of a Python-based simulation environment for photonic integrated circuits (PICs). Laboratory experiments were conducted to characterize the relationship between input optical power, signal strength, noise contributions, and signal-to-noise ratio (SNR) at the photodiode output. Direct-detection results showed an exponential dependence of SNR on input power, with transimpedance amplification improving sensitivity at low powers but saturating at higher powers. Having a transimpedance amplifier after the photodiode showed that the same SNR can be achieved at a lower input power, improving the receiver sensitivity. Coherent reception measurements demonstrated broadly comparable SNR values, with performance shaped by local oscillator noise and the nonlinear response of integrated variable optical attenuators and transimpedance amplifiers. These findings highlighted the critical importance of operating the receiver front-end within its optimal dynamic range.

A modular simulation tool was developed in parallel to model PICs and system-level metrics such as power loss and SNR prior to fabrication, with preliminary simulations giving reasonable power loss and SNR values for a sample satellite feeder link scenario. Initial implementations focused on amplifier components and circuit handling functions, providing the basis for future extensions to modulators and advanced transceiver architectures. Together, the experimental and simulation results emphasize the trade-offs between direct-detection and coherent schemes, and demonstrate the value of accurate modeling for the design of multi-function PIC transceivers in high-throughput optical communication applications.

Contents

1 Statement of Original Authorship **1**

2 Acknowledgements **2**

3 Abstract **3**

List of Figures **5**

List of Tables **6**

4 List of Acronyms **7**

5 Introduction **8**
5.1 State Of The Art . . . 8
5.2 DLR EPIC Team . . . 10

6 Theory **11**
6.1 Optical Communications . . . 11
6.2 Photonic Integrated Circuits (PICs) . . . 13
6.3 PIC Components: KPI and Noise Sources . . . 14
6.3.1 Platform Material . . . 14
6.3.2 Lasers . . . 16
6.3.3 Waveguides . . . 17
6.3.4 Modulators . . . 18
6.3.5 Amplifiers . . . 19
6.3.6 Detectors . . . 21
6.4 Free-Space Channel . . . 22

7 Methodology **24**
7.1 Lab Experiments . . . 24
7.1.1 IM-DD Sensitivity . . . 24
7.1.2 Coherent Sensitivity . . . 25
7.1.3 LO Impact . . . 27
7.2 Simulation Software in Python . . . 27
7.3 Photonic System Architecture . . . 28

8 Results and Discussion **30**
8.1 Lab Experiments . . . 30
8.1.1 IM-DD Sensitivity . . . 30
8.1.2 Coherent Sensitivity . . . 33
8.1.3 LO Impact . . . 36
8.2 Simulation Software . . . 36
8.3 Photonic System Architecture . . . 38

9 Conclusion **39**

10 Appendix **43**

List of Figures

1 Moore's Law for Photonic Integration; The trend shows the increase of the number of components on a single chip through the years, following a similar trend to electronic integration (Smit, Williams, and Tol 2019). 8
2 OSIRIS Cube-ISL optical terminal on La Palma for a FSO measurement campaign (Credit: DLR, CC BY-NC-ND 3.0). 9
3 SFide PIC chip as seen under a microscope, used in the DLR lab for testing new component geometries for isolating wavelengths. Waveguides, ring-resonators, grating couplers can be seen on the chip. 10
4 Evolution of optical communications systems and its potential future developments, showing the information rate increase since 1980 (Miyamoto and Takenouchi 2014). 11
5 Map of undersea fiber optical cables covering the globe to connect continents with high-speed information communication. Dark blue show existing cables, light blue show planned cables (circa 2019) (Saracco 2019). 12
6 OOK modulation scheme constellation, showing the relative distance between the two symbols (each carrying one bit) and that modulation happens in only the real plane (Sabol et al. 2008). 13
7 QPSK constellation diagram, showing the distance between symbols (each representing two bits) and that modulation is represented in two planes, increasing complexity (Camuñas-Mesa and Rosa 2023). 14
8 Table comparing the performance for different properties of PIC platform materials; green meaning excellent, yellow meaning adequate, red meaning poor. 15
9 Schematic diagram of a DFB laser (Mukherjee et al. 2020). 16
10 Schematic diagram of an ECL laser on a PIC chip. The laser cavity is made from using ring resonators R_1 and R_2 as mirrors (Komljenovic et al. 2017). . 16
11 (a) a planar waveguide, used in high power lasers and amplifiers, and (b) a non-planar waveguide, used in optical fibers and interconnect channels (Selvaraja and Sethi 2018). 17
12 Schematic structure of a MZM using a push/pull configuration (Mukherjee et al. 2020). 18
13 Transmitter for PM-QPSK operation, showing four MZMs in the circuit to show the setup for modulating light in I/Q components, for both orthogonal polarizations (Mukherjee et al. 2020). 19
14 Schematic structure of a normal-incident p-i-n photodiode (Mukherjee et al. 2020). 21
15 Experiment setup for investigating the SNR of a COTS OOK transceiver by IM-DD with varying input power. The OOK transceiver is connected to the router in the background, a yellow optical fiber connects the transceiver to the VOA, the VOA then connects to the PD in the foreground, and a blue wire connects the PD output to an oscilloscope. 25
16 Block diagram of circuit for investigating the SNR of a COTS OOK transceiver by IM-DD with varying input power. 25
17 Experiment setup for investigating the SNR of a COTS OOK transceiver by coherent reception with varying input power. 26
18 Block diagram of circuit for investigating the SNR of a COTS OOK transceiver by coherent reception with varying input power. 27

19 PIC circuits for OOK (top) and PM-QSPK (bottom), showing the transmitters and receivers for each operation. 29
20 Signal against Input power for the OOK transceiver using IM-DD reception. . 31
21 Noise against Input power for the OOK transceiver using IM-DD reception. . 32
22 SNR against Input power for the OOK transceiver using IM-DD reception. . . 32
23 SNR against Input power for the OOK transceiver using coherent reception. . 33
24 Signal against receiver board VOA attenuation for the OOK transceiver using coherent reception. 35
25 SNR against receiver board Gain Control Voltage for the OOK transceiver using coherent reception. 35
26 Block diagram of the simphony simulator software logic. Full boxes indicate they are implemented, dashed boxes indicate they are not yet implemented, but planned. Purple boxes indicate 'main'; Orange boxes indicate inputs; Green boxes indicate outputs. 37
27 Block diagram of the simulation software tool logic. Full boxes indicate they are implemented, dashed boxes indicate they are not yet implemented, but planned. Purple boxes indicate 'main'; Orange boxes indicate inputs; Green boxes indicate outputs. 37
28 Example scenario of a feeder link to a satellite in LEO orbit at 50 degrees, showing the expected link budget for an OOK operation. 38

List of Tables

1 Key performance indicators (KPIs) of lasers in photonic integrated circuits. . 17
2 Key performance indicators (KPIs) of waveguides in photonic integrated circuits. 18
3 Key performance indicators (KPIs) of modulators in photonic integrated circuits. 20
4 Key performance indicators (KPIs) of amplifiers in photonic integrated circuits. 20
5 Key performance indicators (KPIs) of detectors in photonic integrated circuits. 22
6 Internal (system) and external (channel) losses/parameters in free-space optical communications for PIC-based FSO links. 23

4 List of Acronyms

CMOS Complementary Metal–Oxide–Semiconductor

COTS Commercial Off-The-Shelf

Cube-ISL Cube-Inter-Satellite Links

DLR German Aerospace Centre

DSP Digital Signal Processing

EPIC Extraterrestrial Photonic Integrated Circuit(s)

FSO Free Space Optical (communications)

IM-DD Intensity-Modulation Direct-Detection

LO Local Oscillator

MZM Mach–Zehnder Modulator

OOK On–Off Keying

OSIRIS Optical Space Infrared Downlink System

PD Photodiode/Photodetector

PIC Photonic Integrated Circuit

PM-QPSK Polarization-Multiplexed Quadrature Phase-Shift Keying

RF Radio-frequency

SNR Signal-to-Noise Ratio

SWaP Size, Weight, and Power

TIA Transimpedance Amplifier

VOA Variable Optical Attenuator

5 Introduction

This report details the work the author has conducted within the Communications and Navigation (KN) Institute of the German National Aerospace Agency (DLR). DLR is the national aeronautics and space research center of the Federal Republic of Germany, with the KN institute being responsible for mission-oriented research in areas such as spacecraft navigation, with a focus on global positioning systems and alternatives in case of outages, and optical and RF telecommunications. The author was embedded into the institute's Extraterrestrial Photonic Integrated Circuits (EPIC) team which focuses on the integration of photonic components onto chips known as photonic integrated circuits (PICs), to increase overall functionality for use in the free-space optical communications. The team investigates the use of PICs in the optical communications aspect of the Osiris CubeISL mission, and the time transfer and synchronization of the Galileo satellite constellation. This is allowed by the concept of 'miniaturization', decreasing the size of existing optical components in telecommunications to fabricate system-on-chip solutions. By fabricating smaller photonic components, more components can be integrated onto chips thereby increasing the functionality, with a trend of number of components per chip following Moore's Law seen also in integrated electronics, shown in Fig. 1.

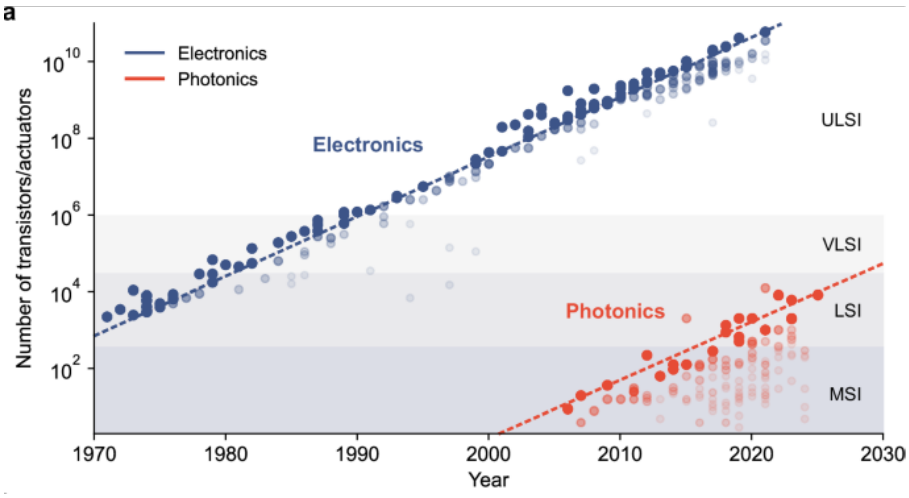


Figure 1: Moore's Law for Photonic Integration; The trend shows the increase of the number of components on a single chip through the years, following a similar trend to electronic integration (Smit, Williams, and Tol 2019).

5.1 State Of The Art

Optical satellite communications have emerged as a key technology for next-generation space networks, driven by the need for higher data rates, reduced spectrum congestion, and secure links, which radio-frequency (RF) systems lack. Unlike conventional RF systems, free-space optical links exploit the high carrier frequency of near-infrared lasers to achieve gigabit-to-terabit throughput with compact, lightweight terminals. Recent demonstrations by ESA's European Data Relay System (Heine et al. 2014), NASA's Lunar Laser Communication Demonstration (Boroson et al. 2014), and commercial operators such as SpaceX's Starlink constellation (Clark 2021) have validated inter-satellite laser links as a practical means to establish global optical networks in orbit. These advances highlight the potential of optical communications to support high-throughput data relay, Earth observation downlinks, and deep-space

missions, while also addressing the challenges of pointing, acquisition, tracking, and atmospheric turbulence mitigation (Toyoshima 2005).
The DLR Optical Space Infrared Downlink System (OSIRIS) program develops optical communications technology and systems for direct downlinks and for connections between small satellites (Fuchs and Schmidt 2019). This programme addresses the need for higher data rates in small spacecraft by researching the employment of optical communications in space. This programme began with the two spacecraft BiROS, which was concluded in 2020, and the still ongoing Flying Laptop, developed by the University of Stuttgart. The optical output from the Flying Laptop spacecraft orbiting at LEO was continuously detected by the ground station in DLR's Oberpfaffenhofen site for 10 minutes in 2018, showing promising results for using optical communications in downlinks. Fig. 2 shows an optical terminal used in a measurement campaign for the OSIRIS Cube-ISL project to investigate the effects of the free-space channel on the signal with the other terminal located 140 km away.



Figure 2: OSIRIS Cube-ISL optical terminal on La Palma for a FSO measurement campaign (Credit: DLR, CC BY-NC-ND 3.0).

Despite these achievements, free space optics (FSO) performance is limited by atmospheric turbulence, fog, precipitation, and dust. These channel properties cause signal attenuation, scintillation, and beam wander. Stringent pointing requirements for narrow optical beams are also a factor for limiting FSO performance (Raj and Majumder 2019). Mitigation strategies include aperture averaging, adaptive optics for wavefront correction, MIMO-based spatial diversity, and hybrid FSO/RF systems for redundancy, along with advanced beam tracking techniques such as a AI-assisted particle swarm optimization (Eguri, Raj A, and Sharma 2022). With the integration of coherent detection, adaptive beam control, and digital signal processing, FSO is expected to play a key role in 6G backhaul, large satellite constellations, and quantum-secure communication. Multi-Tbps wireless links that seamlessly converge with optical fiber infrastructure is an ongoing research topic and is being made possible using PICs (Kumar, Saqib, and Hussain 2024).
PICs have been shown to have many advantages placing them as a suitable alternative to electronic circuits similar systems (Iwai and Ohmi 2002). PICs rely on photons to carry information, allowing data communications to happen at the speed of light. This inherent speed advantage results in uses where high data rate and reduced latency is crucial, such as communication networks and data-intensive computing (Zhao et al. 2017; Doerr 2010). Like electronic integrated circuits, PIC chips are possible due to the miniaturization of components

like waveguides, modulators and lasers. Because of this method, research is being conducted in using PICs in space for free-space optical communications while adhering to size, weight and power (SWaP) requirements.

5.2 DLR EPIC Team

The DLR Extra-terrestrial Photonic Integrated Circuits (EPIC) team is researching the development of PICs for free-space optical communication. This research also includes investigating how suitable PICs are in the harsh space environment, performing radiation modeling on circuits to determine its effect on the PIC operation (Terrasanta, M. W. Ziarko, et al. 2025; Terrasanta, Zinth, et al. 2025). One of the benefits of using PICs is the ability to integrate active and passive components in a compact form factor for use on satellites, where there is a high importance on SWaP requirements. Studies have demonstrated the feasibility of employing a PIC-based solution for high-speed coherent transceivers to deliver high throughput communications between optical satellite links (M. Ziarko et al. 2024; Mata Calvo et al. 2019). Free-space optical transmission feeder links, i.e. ground to satellite links, have also been demonstrated using representative atmospheric turbulence conditions and worst-case conditions simulations (Surof, Poliak, and Calvo 2017; Conroy et al. 2018). Among the research involving simulations discussed previously, the EPIC team conduct laboratory work and experiments using PICs which consist of probing different parts of a sample PIC to understand how each component operates, under what conditions are optimal operations achieved and to test new component geometries. An example PIC used in the DLR optical lab is shown in Fig. 3. The main focus of the SFIDE v1 PIC was on wavelength division multiplexing to maximize the communication throughput, alongside other testing, such as new component geometries for investigating the experimental distance between two waveguides in a coupler to isolate a specific wavelength.

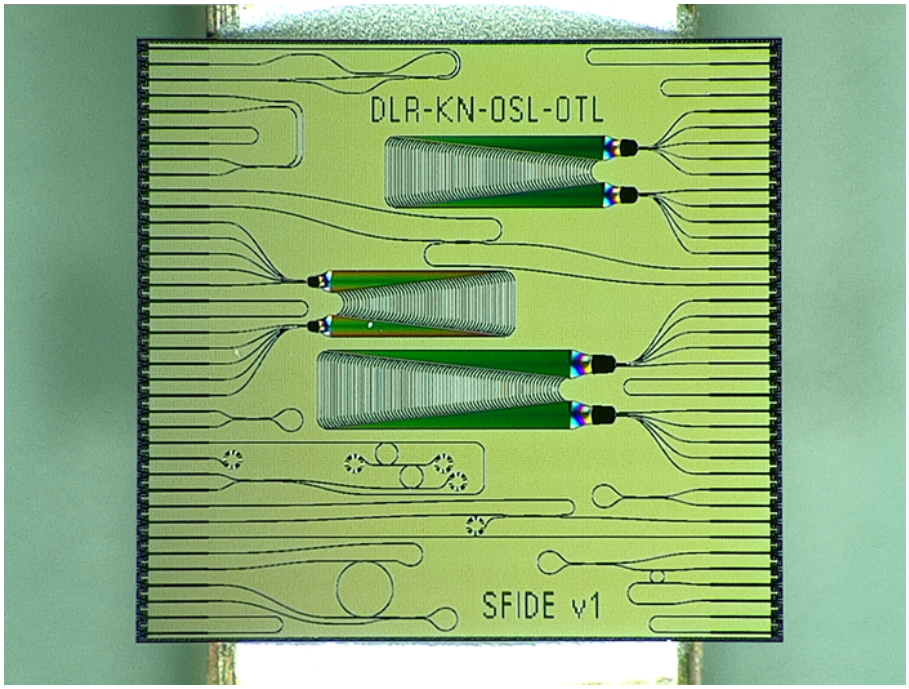


Figure 3: SFide PIC chip as seen under a microscope, used in the DLR lab for testing new component geometries for isolating wavelengths. Waveguides, ring-resonators, grating couplers can be seen on the chip.

6 Theory

This section will discuss the applicable theory for the internship, building on the introduction to focus on the applications of PICs for inter-satellite optical communication links and the research the author has conducted while in the EPIC team. The topics that will be discussed are optical communications and PICs, including their manufacturing, components and key performance indicators.

6.1 Optical Communications

Optical communications refers to the transfer of information using light or optical signals. Compared to electronic communications, optical data communications is a relatively new field of research that is still ongoing. Fig. 4 shows the evolution of the data rate of optical communications systems and its potential future developments. Since 1980, the development of low-loss glass fibers, the main carrier of these light signals, allowed the world to be connected through optical communications (Staelin 2009), shown in Fig. 5. However, research and development began as early as the 1970s (Kikuchi 2016). Optical communications is desirable over other methods such as electronic and radio-frequency (RF) due to its high bandwidth, approximately 1 THz, offering a higher data rate, and its low latency and low energy loss, allowing the propagation of information across larger distances using optical amplifiers, with each amplifier being separated by more than 80km (Staelin 2009). After a distance of 50 km in a wire, the bandwidth of electronic and RF schemes decrease in bandwidth until only 2 MHz (ibid.).

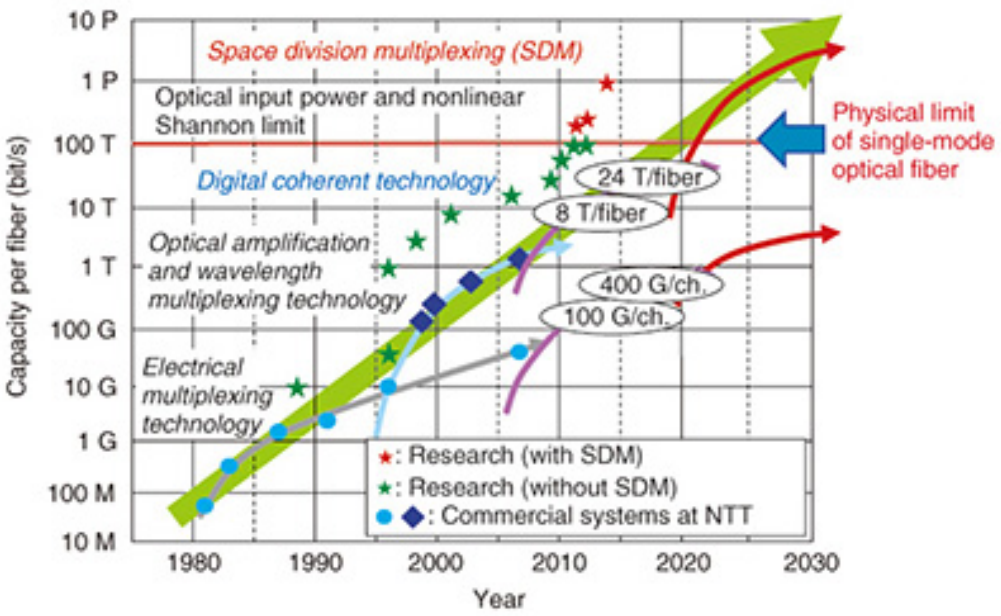


Figure 4: Evolution of optical communications systems and its potential future developments, showing the information rate increase since 1980 (Miyamoto and Takenouchi 2014).

Optical links are not only used for long-distance communication, finding applications in short range links such as in data and artificial intelligence (AI) centers (Burr 2024). Optical communications is especially important for AI development, since AI applications like large-language models and high-performance computing generates a large amount of data (Taubenblatt

2012). This increased amount of data production necessitates the use of optical links for its higher bandwidth demand, its lower latency and its energy efficiency.

Thus, optical communication has been shown to have significant advantages over electronic methods, for example, at long distances and when a higher bandwidth is required. However, it might not be the best solution for every application. One disadvantage of optical communications is its redundancy. Most designers have been hesitant to switch from electronic to optical communications if their current existing and implemented electronic infrastructure already provides the required bandwidth (Farjadrad 2014). Another disadvantage of optical communications is the fragility of optical fibers. These fibers are made from glass and are highly susceptible to damage which will significantly impact its performance. The fragility of optical fibers also causes installation to be highly complex, requiring a larger initial investment and cost than traditional electronic cables. This complexity and fragility also inhibits the optical infrastructure from being able to be reconfigured (AscentOptics 2024).

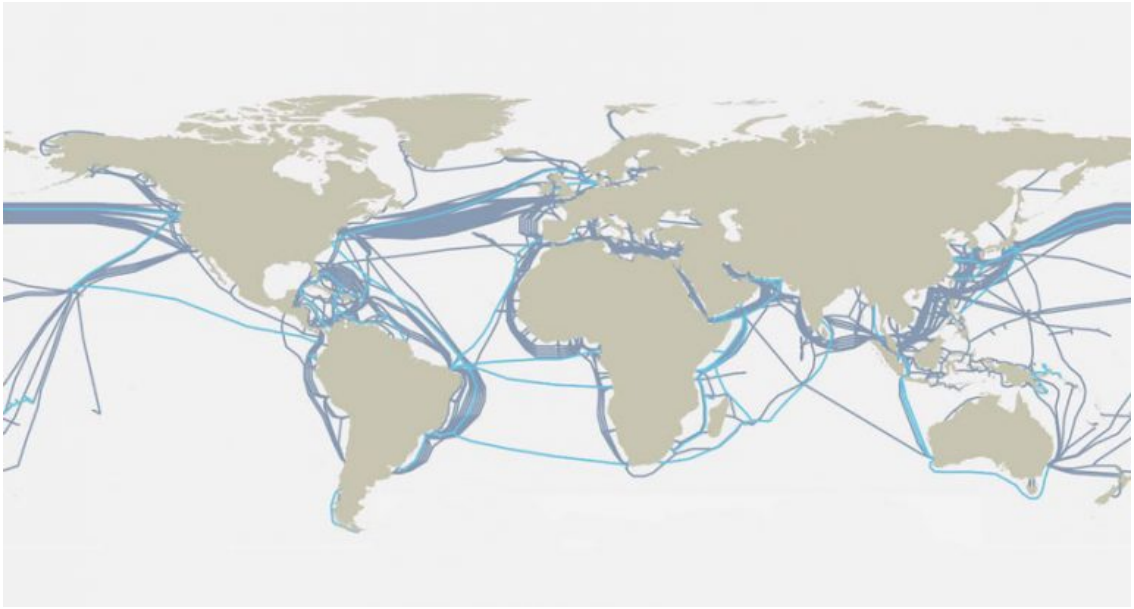


Figure 5: Map of undersea fiber optical cables covering the globe to connect continents with high-speed information communication. Dark blue show existing cables, light blue show planned cables (circa 2019) (Saracco 2019).

Information transfer is done using modulated light signals that change one or more properties of light to encode a signal. The most common properties of light that are modulated are the amplitude, frequency, and phase of the signal. The earliest optical communications involved a system with a transmitter that modulated laser intensity, or amplitude, and a receiver with a photodiode that converts light intensity to a proportional current. This system is known as intensity modulation direct detection (IM-DD), and is still used today due to the receiver's insensitivity to the carrier phase or the state of polarization (SOP) of the signal, which randomly fluctuates during propagation. This system has a limited data rate, however, since the modulation technique transfers only one bit of information in a given pulse duration which depends on the receiver's response time. Constellation diagrams are used to represent modulated signals, displaying them as an XY-plane scatter diagram in the complex plane at symbol sampling instances, i.e. each point on the constellation represents a symbol that is encoded onto the modulated signal (Barrueco et al. 2021). The distance between each point

is representative of how distinguishable the points are, with less distance having a larger error probability at the receiver. On-off keying (OOK) is an example of a modulation technique used in IM-DD, the constellation of which can be shown in Fig. 6. This scheme involves encoding a sentence of binary bits onto a continuous wave, with bit 0 represented as a signal with no amplitude, thus no signal, and bit 1 represented as a signal with some amplitude above a threshold value.

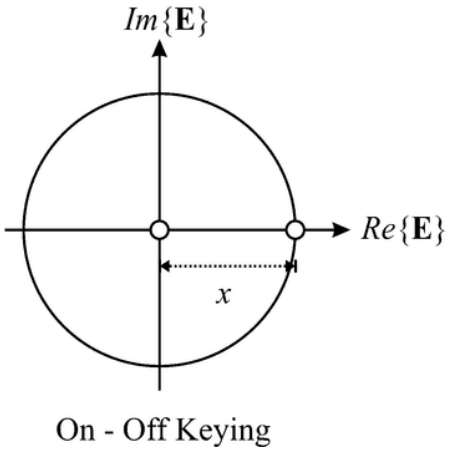


Figure 6: OOK modulation scheme constellation, showing the relative distance between the two symbols (each carrying one bit) and that modulation happens in only the real plane (Sabol et al. 2008).

To achieve a higher data rate, more advanced signal modulation techniques are used, such as polarization mulitplexed-quadrature phase shift keying (PM-QPSK). This technique has the advantage of using more properties of light than OOK to encode information, meaning that more information can be transferred for the same bandwidth compared. PSK differs from OOK by the property of light that is modulated being the phase instead of the amplitude. The constellation diagram for QPSK is shown in Fig. 7. The distance between symbols is larger compared to OOK, showing that PM-QPSK can be more robust to noise and has a lower probability of errors. This constellation diagram represents one polarization, so in a PM-QPSK system, the same constellation diagram applies to the orthogonal polarization, too. The technique modulates both the in-phase (I), or real, and the quadrature (Q), or imaginary, components of the signal to achieve two bits per symbol. Since the same is done to the orthogonal polarization, the data rate increases to 2 bits x 2 polarization, compared to 1 bit x 1 polarization for OOK. The increase in data rate also means a more complex system, both at transmission and at reception. The signal at the receiver must be mixed with another laser, or local oscillator (LO), with known phase and amplitude to allow the signal to be decoded. The addition of a LO means that this receiver is called coherent, whereas IM-DD receivers are known as non-coherent, since only the intensity information is recorded and the phase and polarization are unknown.

6.2 Photonic Integrated Circuits (PICs)

PICs can be thought of as analogous to electronic circuits, with the major difference of using photons instead of electrons as information carriers. Many of the components that can be found on electronic circuits have an equivalent photonic component; for example, waveguides in photonic circuits are electrical wires in electronic circuits; similarly, semiconductor optical

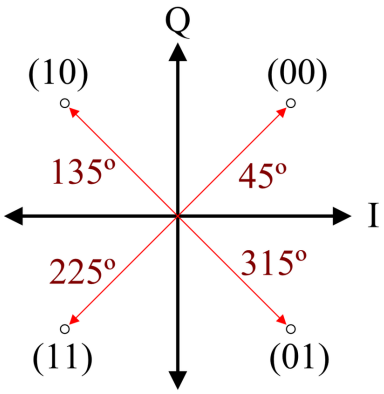


Figure 7: QPSK constellation diagram, showing the distance between symbols (each representing two bits) and that modulation is represented in two planes, increasing complexity (Camuñas-Mesa and Rosa 2023).

amplifiers (SOA) are the photonic transistors (Paschotta 2008). PICs offer many advantages over electronic chips, such as their higher bandwidth and their capability of low thermal effects, a big problem in electronics (Dhumal, Kulkarni, and Ambhore 2023). The ability of PICs to be manufactured using existing processing flows in many foundries allow a high yield, large volume manufacturing and a lower price.

6.3 PIC Components: KPI and Noise Sources

A thorough study was conducted on the different components found on PICs. This study involved looking at the different devices of components and assessing whether they are applicable to the desired output. PIC designs for OOK and PM-QPSK modulation schemes were researched, with emphasis on high-throughput architecture and devices; 10Gbps for OOK, 100Gbps for PM-QPSK. The key-performance indicators (KPI) were evaluated to quantify the performance of the PIC designs for the multi-function transceiver, along with the noise and loss that each component imparts to assess the SNR. The following system KPIs are applicable to estimating the performance of the multi-function transceiver:

- SWaP (size, weight and power)
- SNR (signal-noise ratio)
- Bandwidth
- Complexity

The following subsections discuss specific PIC components and their application in context of light modulation. Their KPIs and noise contribution to the system are evaluated since they will be used in assessing the performance of each PIC simulated using the simulation tool.

6.3.1 Platform Material

The components of a PIC are placed or etched onto the platform material. Different chip elements and devices required different semiconductor material layers. These layers are grown on the base semiconductor wafer through a process called epitaxy, or deposited by physical or chemical vapor deposition. A mask of the circuit layout is used to imprint the design onto the semiconductor wafer in a process known as projection optical lithography. The material

that is not covered by the mask is etched away using either ion bombardment for anisotropic etching or immersion of the material in a liquid reactant for isotropic etching. The wafer is then cleaned and prepared by means of methods such as passivation, planarization, and metallization (EffectPhotonics 2023).
The materials on which PICs are fabricated are:

- InP (indium phosphide)
- SoI (silicon-on-insulator)
- Si_3N_4 (silicon nitride)
- SiO_2 (silicon dioxide)
- $LiNbO_3$ (Lithium Niobate)
- Polymer

Each material has its advantages and disadvantages in certain aspects, such as increased propagation loss or its compatibility with complementary metal-oxide-semiconductor (CMOS) technology. InP was the most common material on which to fabricate PICs because it is the only platform material that is a semiconductor, which means that lasers can easily be integrated into the material (Klamkin et al. 2018). All the other base materials require an external laser to input light into their circuit, usually InP or GaAs lasers. Now Silicon based materials dominate the PIC market, due to its transparency and high refractive index in the near-infrared spectrum, as well as the mature fabrication of CMOS technological stack in foundries (Vyshnevyy et al. 2023). InP also allows the integration of active components other than lasers, such as semiconductor optical amplifiers, photodetectors and modulators. Thus, many manufacturers prefer InP for its 'all-in-one' solutions. However, one disadvantage of InP over the other materials is its incompatibility with CMOS technology, necessitating intermediate materials to bind the technology onto the base (Goswami et al. 2024).

PROPERTY	InP	SoI	Si_3N_4	SiO_2	$LiNbO_3$	Polymer
Loss						
Optical Gain/Amplification						
Photodiodes						
Fibre Coupling						
Spectral Range						
Polarisation Independence						
RF Modulation						
CMOS Compatibility						
Durability						
Footprint						
All-in-one						
Open Access MPWs						

Figure 8: Table comparing the performance for different properties of PIC platform materials; green meaning excellent, yellow meaning adequate, red meaning poor.

Fig. 8 shows a comparison of the base materials in terms of the different properties they offer. Silicon, the main wafer material in electronic circuits, can also be used in photonics. The table shows that silicon-based materials not only offer excellent CMOS integration but also improve on waveguide propagation losses, for example. So, although InP has been widely

used as the sole material in PIC chips, there is motivation to use multiple materials to access a wider array of advantages. However, this leads to other losses, such as chip edge-coupling loss due to a mode mismatch when entering a new medium (Zhu et al. 2023). PIC designers must consider whether the improved losses induced by the material outweigh the loss and coupling complexity from the component-platform interface.

6.3.2 Lasers

Lasers are used to send photons into a circuit. Lasers are devices that emit light through stimulated emission of electromagnetic radiation, occurring when a photon causes an excited electron to relax and emit two identical photons. Lasers consist of a gain medium in which stimulated emission occurs, and a pump current which begins the lasing action. This gain medium and pump apparatus is positioned in the cavity between two mirrors, and laser types are categorized by the cavity structure (Mukherjee et al. 2020). The types of lasers commonly found in PICs are:

- Distributed Feedback (DFB) Laser (Fig. 9.)

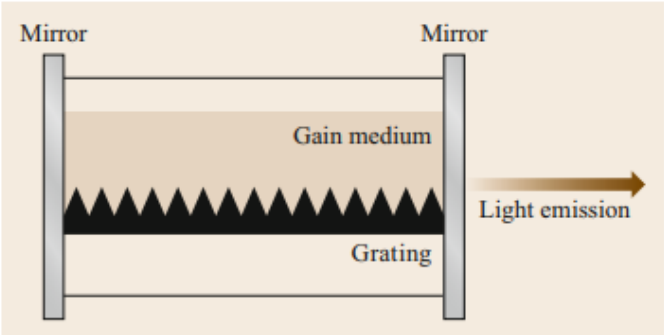


Figure 9: Schematic diagram of a DFB laser (Mukherjee et al. 2020).

- External Cavity Laser (ECL) (Fig. 10.)

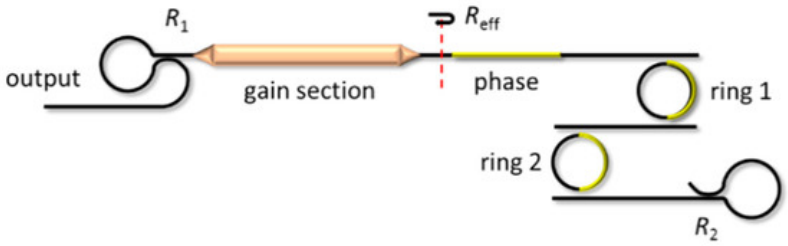


Figure 10: Schematic diagram of an ECL laser on a PIC chip. The laser cavity is made from using ring resonators R_1 and R_2 as mirrors (Komljenovic et al. 2017).

The main advantage of using lasers in photonic integrated circuits (PICs) compared to conventional light sources like light bulbs is the coherence and spectral purity of the emitted light. Lasers produce narrow-linewidth, phase-stable beams that are well-suited for high-speed optical communications, where minimal losses and reliable phase encoding are essential (Eldada 2004). By contrast, light bulbs emit broadband, incoherent light in all directions, which makes them unsuitable for such applications. More generally, while other types of non-semiconductor

light sources (such as gas or solid-state lasers) can also generate coherent beams, the integration of semiconductor lasers or LEDs directly onto PICs provides additional benefits of compactness, scalability, and efficient coupling into on-chip waveguides.
The key performance metrics and noise sources for lasers in PIC simulators are shown in Table 1 (K. 2011).

KPI (Lasers)	**Brief Definition**
Performance Metrics	
Linewidth	Spectral purity; narrow linewidth improves coherence.
Power Consumption	Electrical power required for laser operation.
Output Power	Optical power emitted from the laser.
Tunability	Ability to adjust emission wavelength over a range.
Noise Metrics	
Phase Noise	Frequency fluctuations of the laser output.
Thermal Noise	Noise from heating effects and drive electronics.
Relative Intensity Noise (RIN)	Fluctuations in output optical intensity.

Table 1: Key performance indicators (KPIs) of lasers in photonic integrated circuits.

6.3.3 Waveguides

Waveguides are the components of PICs that guide light between the different circuit elements of a PIC, and is defined as any structure that's used to guide the flow of an electromagnetic wave in a direction parallel to its axis. They are analogous to interconnects in an integrated electronics circuit, and behave similarly to optical fiber cables. Waveguides guide light using the principle of total internal reflection, in which the light wave is reflected back within the waveguide upon contact with the edge of the guide. To facilitate this behaviour, waveguides are constructed with an inner core material that has a larger refractive index than the outer cladding material.

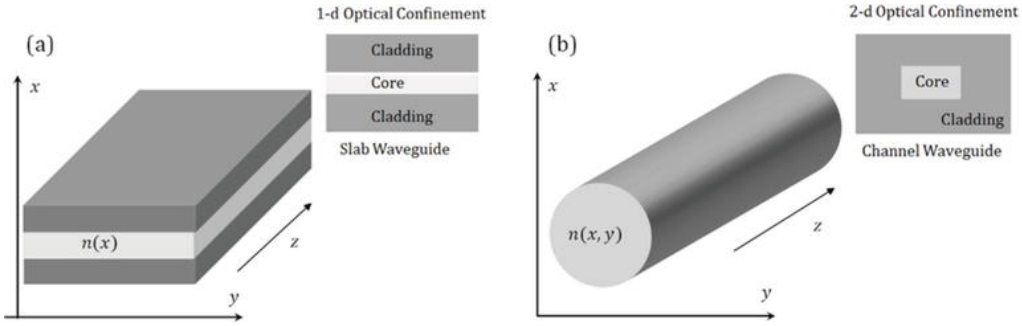


Figure 11: (a) a planar waveguide, used in high power lasers and amplifiers, and (b) a non-planar waveguide, used in optical fibers and interconnect channels (Selvaraja and Sethi 2018).

Waveguides can be classified on the basis of their geometry, mode propagation, refractive index distribution, and material platform. The effect of the waveguide material on the light beam has been previously discussed and is shown in Fig. 8. Waveguides can be confined in 1- or 2-dimension optical confinement geometries, also known as planar and non-planar, where

the core is surrounded by cladding along one direction and where the core is surrounded on all sides, shown in Fig. 11. PICs typically use a both planar waveguides, since they are primarily used for high-power lasers and amplifiers, and more commonly non-planar waveguides, which are used for channels connecting different optical components. PIC waveguides are guided mode waveguide, meaning total internal reflection occurs at both boundaries and minimal light is radiated to the cladding material. The dimensions of the waveguide determine the modes that can propagate within a waveguide. Typically, waveguide dimensions are such that only a single mode oscillates in the waveguide because there is less propagation loss and narrower linewidth than a multi-mode waveguide. Single-mode waveguides can also be scaled down further than multi-mode guides since the core must be small enough that only a single mode can oscillate, optimal for PIC fabrication and performance.
Since waveguides are passive components, they do not introduce noise into the system. The key performance indicators for waveguides are shown in Table 2.

KPI (Waveguides)	**Brief Definition**
Performance Metrics	
Propagation Loss	Optical power loss per unit length of the waveguide (dB/cm).
Waveguide Type	Waveguide geometry and material platform (e.g., strip, rib, slot; silicon, SiN, InP).

Table 2: Key performance indicators (KPIs) of waveguides in photonic integrated circuits.

6.3.4 Modulators

Modulators are electro-optic components that manipulate a property of the light beam using an electrical signal. Modulators are categorized based on the parameter of light that they modulate, or on the mechanism by which modulation is achieved. For example, modulation can be done by direct-modulated lasers, where the laser itself acts as a modulator and the power output is controlled by the pump current, or by electro-absorption modulators, where the material absorption spectrum is changed by an applied electrical field, causing a delay in phase (Mukherjee et al. 2020). These examples are used to modulate the power of the light signal so they are typically found in OOK circuits.

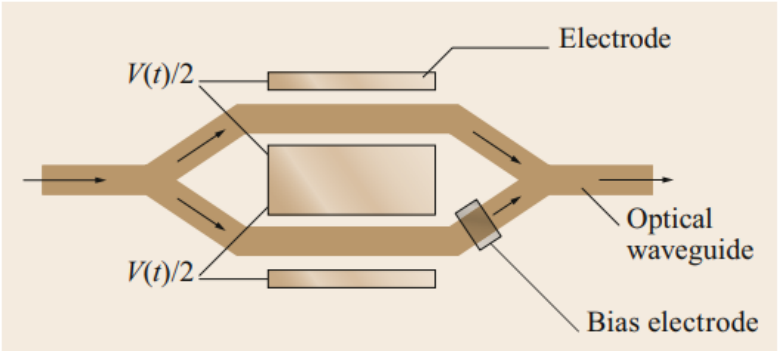


Figure 12: Schematic structure of a MZM using a push/pull configuration (Mukherjee et al. 2020).

In PM-QPSK operations, the phase of light is modulated to encode information. A Mach-Zender modulator (MZM) shown in Fig. 12 is an electro-optic device and is the most common

device for phase modulation, though it can also be used for amplitude modulation. The power ratio between the maximum and minimum modulated optical power is known as the extinction ratio, and is an important figure of merit for modulators since the data reception relies heavily on the separation of different power levels. The MZM splits the light into two equal length arms, delays the phase through one of the arms and then recombines the two paths at the output. The phase of the light beam is modulated by inducing a potential difference across a waveguide which causes the carrier density in the semiconductor material to vary, acting to change the effective refractive index the optical wave experiences. The $V\pi$ parameter is the voltage needed to introduce a phase delay of π. The most common MZM configuration is known as a push-pull MZM where the two arms have equal voltages but opposite signs to nullify modulation chirps, which act to broaden the spectral bandwidth and degrade the signal as it propagates through dispersive media. The transmitter shown in Fig. 13 of a PM-QPSK transceiver employs four MZMs to create the encoded light signal, two pairs of MZMs modulating the I and Q components for both X and Y polarizations, which is then combined at the output using a polarization beam combiner (PBC). In the past, bulk $LiNbO_3$ modulators have been used in traditional commercial line-side optical transmitters which have a footprint of typically 5-7 cm. Nowadays, MZMs are used on chips to decrease the footprint. Smaller modulators are being researched for use in PICs, with studies showing modulators made from other materials such as InP and SiPh having a smaller footprint while maintaining similar performance as larger modulators (Ogiso et al. 2017).

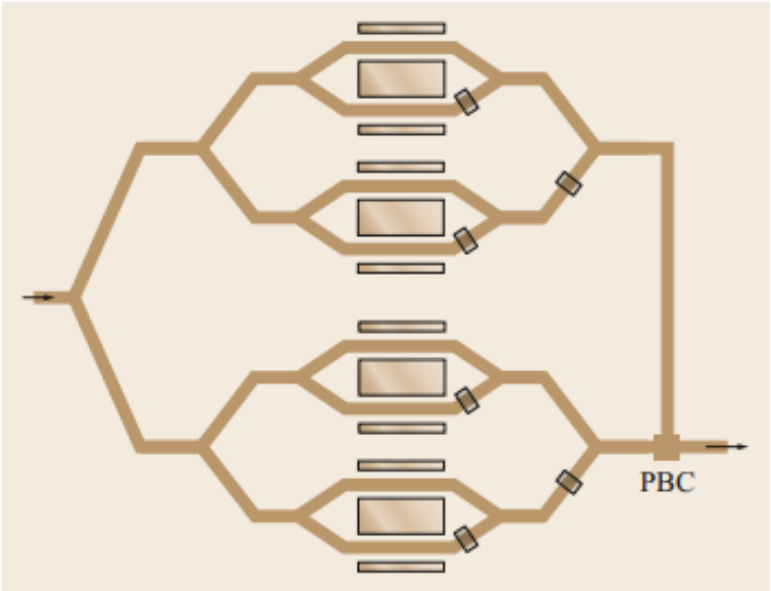


Figure 13: Transmitter for PM-QPSK operation, showing four MZMs in the circuit to show the setup for modulating light in I/Q components, for both orthogonal polarizations (Mukherjee et al. 2020).

The figures of merits for MZMs are shown in Table 3 (Mukherjee et al. 2020).

6.3.5 Amplifiers

Amplifiers in PICs are essential components used to compensate for the optical losses introduced by waveguides, couplers, and modulators, enabling longer transmission distances and higher system performance. The most common type is the semiconductor optical amplifier

KPI (Modulators)	Brief Definition
Performance Metrics	
Bandwidth	Maximum modulation speed supported (GHz).
Vπ	Voltage required for a π phase shift.
Insertion Loss	Optical power lost due to the modulator.
Extinction Ratio	Contrast between logical '1' and '0' optical levels.
Footprint	Physical size of the modulator on the PIC.
Noise Metrics	
Phase Noise	Drive voltage fluctuations imprinted as phase noise.
Thermal Noise	Noise from resistive heating and drive electronics.

Table 3: Key performance indicators (KPIs) of modulators in photonic integrated circuits.

(SOA), which provides gain through stimulated emission in a semiconductor medium, allowing direct integration with other active and passive photonic devices. While SOAs offer compactness and electrical tunability, they also introduce noise in the form of amplified spontaneous emission (ASE), which degrades the SNR and must be considered in system design. Other amplification approaches, such as erbium-doped waveguide amplifiers, are less common in PICs due to integration challenges but remain relevant as standalone optical components, such as amplifying a transmitted signal to compensate for the losses incurred by the free-space channel.
In addition to optical amplifiers, electronic amplifiers are also used in conjunction with PICs. In transmitter PICs, a digital-analog convert (DAC) is needed to convert a binary series to a continuously time-varying voltage which operates on the light beam through electro-optic modulators. The voltage generated from the DAC may be too small for the modulator to optimally function. A linear driver amplifier is used between DACs and modulators to amplify the voltage to an optimum level. In PIC receivers, the electrical signal after a photodetector is typically small, and must be boosted before it can be decoded by digital signal processing (DSP). A low-noise transimpedance amplifier (TIA) follows a PD to convert the current I_{ph} generated from photons to a proportionate output voltage V_{pp}. TIAs are characterized by their transimpedance Z, which governs the conversion proportion by Ohm's Law V_{pp} / I_{ph}. Table 4 shows the KPIs for amplifiers in PICs.

KPI (Amplifiers)	Brief Definition
Performance Metrics	
Gain	Signal amplification (dB).
Saturation Power	Input level for gain compression.
Polarisation Insensitivity	Stable performance vs. polarisation.
Power Consumption	Electrical power requirement.
Maximum Output Power	Highest usable optical output.
Noise Metrics	
Noise Figure	Added noise from ASE.
Thermal Noise	Noise from resistive heating and drive electronics.

Table 4: Key performance indicators (KPIs) of amplifiers in photonic integrated circuits.

6.3.6 Detectors

Detectors in PICs enable the conversion of optical signals into electrical currents through the process of photon absorption followed by electron-hole pair generation, allowing for information retrieval and system monitoring within integrated platforms. The most common type is the photodiode (PD), typically based on germanium or III–V semiconductors integrated with silicon waveguides, offering high responsivity and compatibility with standard CMOS processes, in the case of germanium. Key performance parameters include responsivity, dark current, bandwidth, and noise equivalent power, which together determine detection efficiency and signal fidelity. Detectors in PICs must balance sensitivity and speed while maintaining low noise and compact footprints, making them essential for applications ranging from optical communication and sensing to emerging fields such as quantum photonics.

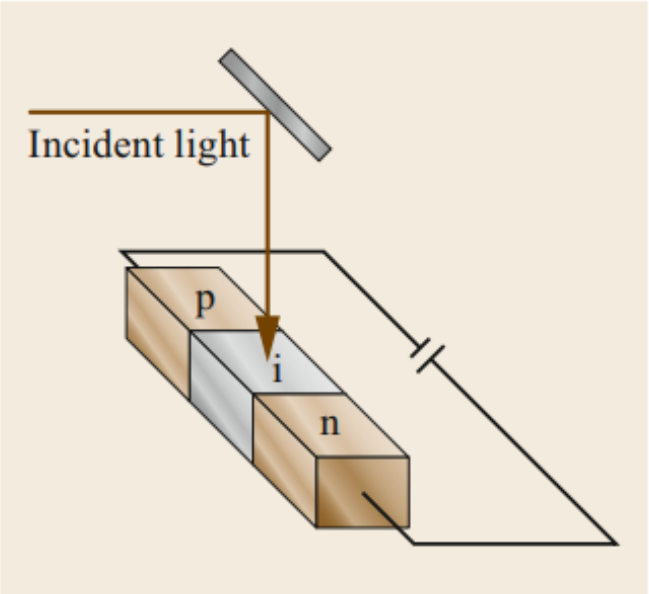


Figure 14: Schematic structure of a normal-incident p-i-n photodiode (Mukherjee et al. 2020).

In photonic integrated circuits (PICs), the most widely used photodetectors (PDs) are p–i–n photodiodes, with avalanche photodiodes (APDs) not as common due to their high bias voltage which is not always possible on PICs. P–i–n photodiodes, shown in Fig. 14 consist of an intrinsic semiconductor layer between a p-doped and n-doped semiconductor layers, and operate by a reverse bias being applied to the p-n junction which sweeps charge carriers to the contacts, which appear as photocurrent. They provide high responsivity, low dark current, and compatibility with CMOS processes, though with a trade-off in bandwidth, making them the standard choice for high-speed optical communication (Lucovsky, Schwarz, and Emmons 1964). APDs, on the other hand, offer internal gain through impact ionization, which enhances sensitivity for detecting weak optical signals, though at the cost of higher noise and more complex biasing requirements. Emerging detector technologies such as metal–semiconductor–metal (MSM) detectors and superconducting nanowire single-photon detectors (SNSPDs) are also being explored in PICs for ultrafast detection and quantum applications (Cheng et al. 2014; Steinhauer, Gyger, and Zwiller 2021).
The KPI and noise sources for PDs are shown in Table 5.

KPI (Detectors)	Brief Definition
Performance Metrics	
Quantum Efficiency	Ratio of detected photons to incident photons.
Responsivity	Relates optical input to generated current (A/W).
Response Time	Speed of detector response.
Bandwidth	Defines maximum modulation frequency that can be resolved.
Dark Current	Current generated without illumination.
Noise Metrics	
Shot Noise	Statistical fluctuations from discrete photon/electron arrivals.
Thermal Noise	Resistive heating noise in the detector and readout circuitry.
Burst Noise	Low-frequency fluctuations due to random trapping and release of charge carriers.

Table 5: Key performance indicators (KPIs) of detectors in photonic integrated circuits.

6.4 Free-Space Channel

The free-space channel in FSO telecommunications refers to the portion of the communication link where an optical signal propagates through the atmosphere without the guidance of a fiber or waveguide. In the context of PICs, efficient coupling between on-chip optical sources, such as lasers, and free-space beams is essential for enabling compact and scalable FSO transceivers. The free-space channel introduces unique challenges compared to fiber links, including atmospheric absorption, scattering, turbulence, and beam divergence, all of which introduce losses and act to decrease the signal power at the receiver. Systems can help mitigate these effects through the integration of beam-shaping elements, such as grating couplers or micro-lenses, which allow precise control over beam direction, divergence, and polarization, or through the use of preamplifiers to boost the signal strength before the beam is launched into the channel.
Thus, the free-space channel introduces losses that can be grouped into internal and external losses. Internal losses are concerned with the FSO system, while external losses relate to the channel itself. Table 6 shows the internal and external parameters related to FSO that impact the signal strength (Al-Gailani et al. 2021). The basic principles of FSO through a free-space channel from one PIC transceiver to another are as follows; A PIC transmitter routes light from an on-chip or external laser through a modulator and power monitor to a grating or edge coupler, which launches a collimated beam via an integrated spot-size converter into the free-space channel. Pointing/ATP (acquisition, tracking, pointing) maintains beam alignment while the atmosphere imposes turbulence, absorption, and scattering. At the receiver, a collection aperture / lens focuses the beam onto an in-coupler spot-size converter, which guides light to on-chip filters/splitters and finally to a photodiode(s).

Parameter	Brief Definition
Internal / System Losses and Parameters	
Link margin	Power budget headroom after deterministic losses..
Transmitted power and detector sensitivity	Launched optical power and the minimum input needed at the receiver for a target bit-error rate; together set the achievable link budget.
Transmission bandwidth and wavelength	Receiver/electronics bandwidth (impacts noise) and choice of optical wavelength/window affecting absorption/scattering and eye-safety.
Geometrical losses	Beam spreading vs. aperture capture (depends on divergence θ, path length l, and receive aperture area); reduces received power with range.
Alignment losses	Mispointing/boresight error (e.g., building sway) causing underfill/offset at the aperture; mitigated by automatic pointing and tracking (ATP).
External / Channel Losses (Atmospheric/Environmental)	
Rain	Predominantly non-selective scattering by large drops; attenuation modeled via power law $\gamma_{\text{rain}} = kR^{\alpha}$ and depends on rain rate/climate zone.
Haze	Mie scattering by aerosols such as dust and smoke; reduces visibility, causing steady attenuation dependent on wavelength-/visibility.
Fog	Dense droplets (Mie regime) causing very high attenuation; commonly modeled from visibility (e.g., Kruse/Kim models (Sree Madhuri, Immadi, and Venkata Narayana 2020)).
Atmospheric turbulence	Refractive-index fluctuations producing scintillation, beam wander, and fades; strength characterized by Rytov variance σ_R^2.
Molecular absorption and scattering	Wavelength-dependent gas absorption and Rayleigh/Mie scattering; channel transmittance $\tau = \exp[-\gamma(\lambda)L]$.

Table 6: Internal (system) and external (channel) losses/parameters in free-space optical communications for PIC-based FSO links.

7 Methodology

This section discusses the work conducted by the author within the EPIC team. The goal during this internship is to model a PIC transceiver which has multiple functions, such as containing both OOK and PM-QPSK modulation techniques. The work carried out in the initial weeks involved reviewing the literature and becoming familiar with PICs and existing resources to ultimately deliver the objective of this internship. Part of this work included conducting lab experiments using commercial-off-the-shelf transceivers to investigate the signal-to-noise ratio (SNR) of the circuit as a function of the input optical power. This helped to better quantify the optical power required for the minimum SNR at the detector output for the digital signal processing algorithms to reliably decode the signal.
Ongoing work toward the goal involved investigating different types of software to be able to construct PICs and simulate their power, SNR, as well as noise and loss sources. The goal is to design one or more multifunction PICs that can be applied to inter-satellite links, and to feeder links to satellites in LEO, MEO or GEO orbit. This simulation tool needs to reliably assess the power loss and SNR across components, taking into account all loss and noise each component adds to the system, and to calculate these parameters at the photodetector output. The tool should be easy to use, since multiple PICs will be designed. A scale to grade each circuit will be evaluated and ranked in terms of the system KPI's (see 6.3).
The architecture for the PIC design was researched in parallel with the work conducted in the simulation tool. The modulation schemes that were to be incorporated onto a single chip are OOK and PM-QPSK, with potential of extending the functionality to more modulation schemes. The desire was to have high-throughput modulation schemes, so a study was conducted of existing literature on the components and materials that were used in high-throughput circuits; 10Gbps for OOK, 100Gbps for PM-QPSK. The data rates for these schemes are chosen based on the ESA standards from the ESA Specifications for Terabit/sec Optical Links (ESTOL) document (JAXA and Industries 2024). These system architectures were a way to visually represent the photonic circuits, and were used in conjunction with the simulation tool to investigate the operation of those architectures by examining the output KPI's.

7.1 Lab Experiments

The author was involved in conducting lab experiments in the KN institute's optical lab. These experiments were focused on investigating the performance of COTS OOK transceivers by varying the circuit parameters, such as gain and attenuation, and examining the signal using an oscilloscope. The following subsections describe the experiments conducted, including their setup and components.

7.1.1 IM-DD Sensitivity

This experiment examined the signal power, noise power, and SNR of the OOK transceiver in relation to the photodetector input power. Fig. 15 shows the experimental setup, and a block diagram of the experiment circuit is shown in Fig. 16. The FS 1000BASE-ZX transceiver housed a DFB single-mode laser that operated at a nominal wavelength of 1550nm, which was verified by beating the signal against an LO at 1550nm and observing the beat frequency, with a lower frequency meaning a closer match. The transceiver was plugged into a TP-link Omada router which sent out a repeating arbitrary bit sequence. The bit sentence was irrelevant, only how the transceiver encoded this message optically using OOK. A single-mode fiber connected the transceiver output to a Thorlabs V1000PA variable optical attenuator (VOA) to allow the

input power at the Thorlabs DET08CFC/M photodetector (PD) to be varied by adjusting the voltage. The PD output connected to a Keysight DSA-Z 634A oscilloscope, with one output connecting through a Femto HSA-X-I-2-40 transimpedance amplifier (TIA) and one output without a TIA to investigate the impact of an amplifier on the SNR.

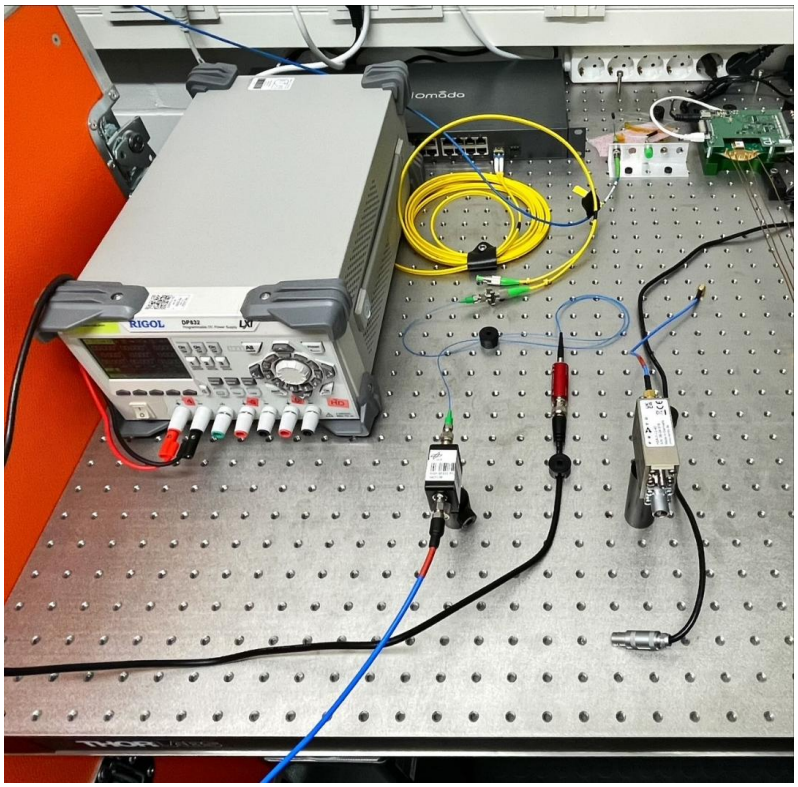


Figure 15: Experiment setup for investigating the SNR of a COTS OOK transceiver by IM-DD with varying input power. The OOK transceiver is connected to the router in the background, a yellow optical fiber connects the transceiver to the VOA, the VOA then connects to the PD in the foreground, and a blue wire connects the PD output to an oscilloscope.

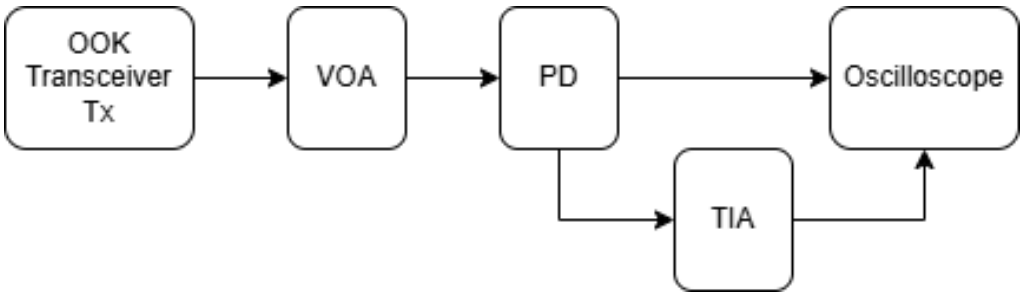


Figure 16: Block diagram of circuit for investigating the SNR of a COTS OOK transceiver by IM-DD with varying input power.

7.1.2 Coherent Sensitivity

A second experiment involving the OOK transceiver was done using a coherent receiver to compare the difference in SNR of both detection methods. A figure of the setup is shown in Fig. 17, with a block diagram shown in Fig. 18. As in the previous experiment, the

transceiver is plugged into a router generating an arbitrary bit sequence. The transceiver output is connected to the VOA to vary the input power at the receiver. In this setup, an LO centered at 1550 nm is interfered with the signal from the transceiver. This is done not only to add gain to the signal to increase the signal power, but to also preserve the phase and polarization information of the signal. Because the transceiver is emitting an amplitude modulated signal, the phase information is not critical to decoding the signal; however, the polarization will shift slightly as the light propagates through the fibers, meaning if the receiver was detecting at only one polarization, some information will be lost. The coherent receiver used was the NeoPhotonics OIF Class 40 for its relatively large bandwidth of 40 GHz and its integration with the PurePhotonics receiver board, allowing users to control and monitor the output of the coherent receiver with the provided GUI software. Within the software, parameters such as gain and VOAs were adjusted for a maximum SNR output. The four outputs of the receiver board corresponded to the in-phase and quadrature components of the signal at the two orthogonal polarizations. Since the information isn't encoded onto the signal phase, the bit sequence can be decoded by doing a root-sum-square operation, shown in Eq. (1) where y is the combined waveform and x_i is output 'i' of 'N' total outputs.

$$y = \sqrt{\sum_{i=1}^{N} x_i^2} \tag{1}$$

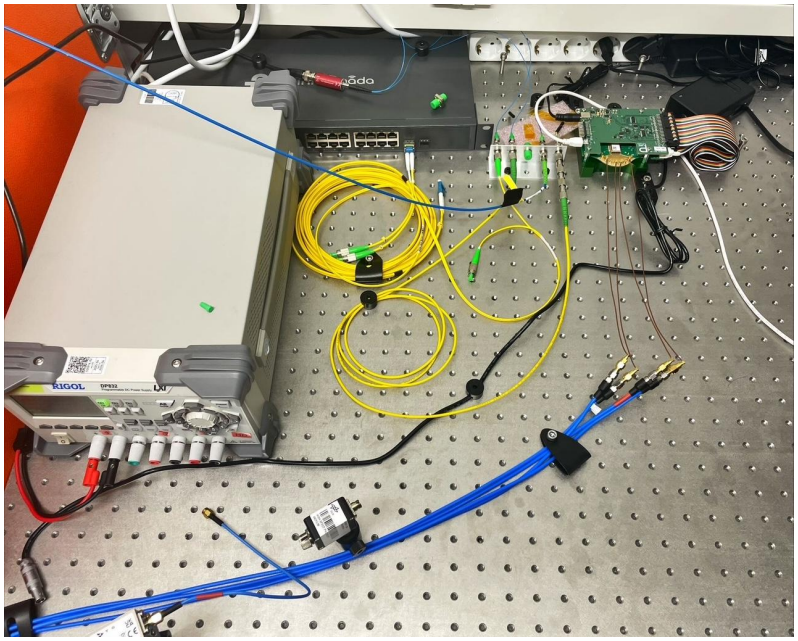


Figure 17: Experiment setup for investigating the SNR of a COTS OOK transceiver by coherent reception with varying input power.

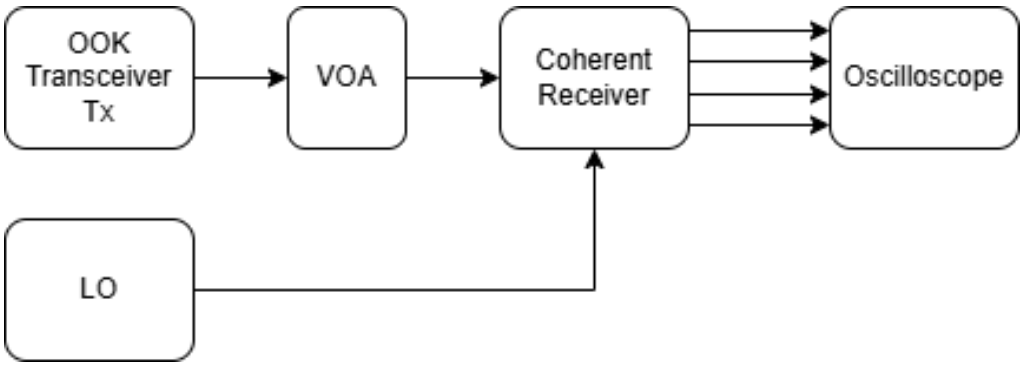


Figure 18: Block diagram of circuit for investigating the SNR of a COTS OOK transceiver by coherent reception with varying input power.

7.1.3 LO Impact

The impact that an LO has on a coherent receiver was investigated. The setup was the same as in the coherent sensitivity shown in Figs. 17 and 18. While maintaining a constant input power of 2 dbm from the transceiver, the power of the LO laser was varied to examine its impact on the SNR. The LO increases the signal power though it also adds laser-related noises such as RIN, phase noise, and shot noise. This experiment determines the optimum power to operate the LO with to achieve the highest SNR.

7.2 Simulation Software in Python

A simulation software is a tool used to extract an expected output by numerical analysis. In the context of PICs, they provide a virtual environment for designing, modeling, and analyzing the behaviour of complex optical devices before fabrication. These tools combine electromagnetic solvers, such as finite-difference time-domain and beam propagation methods, with circuit-level simulators that model waveguides, modulators, lasers, and detectors in an integrated layout. PIC simulation platforms help optimize component geometries, material choices, and coupling strategies while reducing development cost and risk by enabling designers to predict performance metrics such as insertion loss, bandwidth, dispersion, and crosstalk.
One of the tasks for this internship was to prepare a simulation software to test out different designs for the multi-function transceiver. A separate GitLab repository was set up for this task and is regularly updated with code and explanations on the current state of the simulation software and future plans. The software was written in Python and used the Simphony library (Ploeg, Gunther, and Camacho 2021). Simphony is an open-source Python library developed and maintained by members of CamachoLab at Brigham Young University which allows you to define photonic circuits and then run simulations on them. It simulates circuits by first defining the models, or components, in the circuit, and then defining the connections between the components. It simulates the defined circuits by propagating scattering (S-)parameters through the circuit, and numerically calculating the output at the end of the circuit. S-parameters are a frequency-domain way of explaining how light entering a photonic component leaves through its ports, essentially assuming components as black-box building blocks and numerically solving the vector of a complex outgoing wave (b) by multiplying the complex incoming wave (a) with the scattering matrix (S) that is given by the component parameters.

Eq. (2) defines the vectors of the complex incoming and outgoing waves at a photonic

component for 'N' ports. The relation between the incoming and outgoing waves is given by multiplying the incoming wave by the scattering matrix of the component, shown in Eq. (3).

$$\mathbf{a}(\omega) = \begin{bmatrix} a_1(\omega) \\ \vdots \\ a_N(\omega) \end{bmatrix}, \qquad \mathbf{b}(\omega) = \begin{bmatrix} b_1(\omega) \\ \vdots \\ b_N(\omega) \end{bmatrix}. \tag{2}$$

$$\mathbf{b}(\omega) = \mathbf{S}(\omega)\,\mathbf{a}(\omega). \tag{3}$$

The single matrix entry S_{ij} is the complex transfer coefficient for the behaviour of the wave as it enters port 'j' of the component and exits through port 'i'. This is given by the ratio of the transfer from input 'j' to output 'i' at angular frequency 'ω', shown in Eq. (4). The S-parameter is obtained from assuming that no other ports 'k' of the component have an input and that 'j' is the only port that is illuminated.

$$S_{ij}(\omega) \equiv \frac{b_i(\omega)}{a_j(\omega)} \,\Bigg|\, a_k(\omega) = 0 \;\; \forall\, k \neq j. \tag{4}$$

The S_{ij} S-parameter can give information about the amplitude and phase of the signal at port 'i'. Eqs. (5) show that the power of the incoming or the outgoing wave is calculated by squaring the specific port parameter of the wave vector given that the ports are power-normalised, with Eq. (5c) giving the fraction of launched power at 'j' that exits at 'i'. The phase shift of the wave accumulated from port 'i' to port 'j' is obtained by the taking the argument of S_{ij}, which can be used to assess the timing/dispersion and the interference conditions of the wave.

$$P_i^{\text{in}}(\omega) = |a_i(\omega)|^2, \tag{5a}$$

$$P_i^{\text{out}}(\omega) = |b_i(\omega)|^2, \tag{5b}$$

$$|S_{ij}(\omega)|^2 = \frac{P_i^{\text{out}}(\omega)}{P_j^{\text{in}}(\omega)}. \tag{5c}$$

7.3 Photonic System Architecture

The multi-function transceiver should be capable of at least OOK and PM-QPSK operation, with potential of adding additional functionality, such as time-transfer and quantum key distribution. According to the key performance indicators for the system, the ideal solution would have minimal SWaP requirements, sufficient SNR according to DSP requirements, sufficient bandwidth for optimum component performance, and minimal complexity. A circuit that can accommodate data rate of 10 Gbps and 100Gbps for OOK and PM-QPSK operation will be designed while also adhering to the requirements for the ideal solution mentioned previously. To begin designing the multi-function PIC, individual circuits for OOK and PM-QPSK were researched and a basic circuit for both can be found in Fig. 19. The basic circuits show similar components to each other, such as an MZM and spot size converters, meaning that the complexity and SWaP requirements can be minimised if the two circuits are integrated and share components.

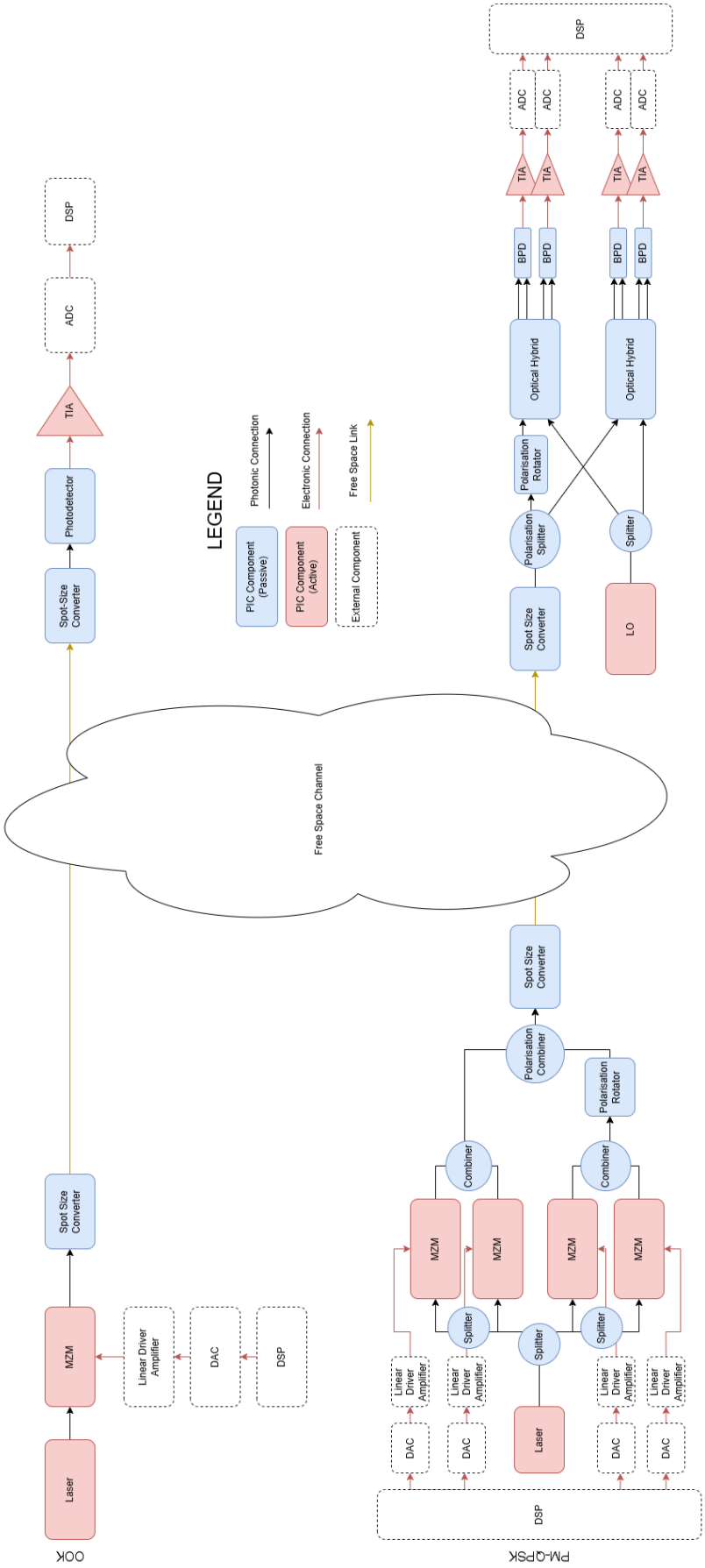


Figure 19: PIC circuits for OOK (top) and PM-QSPK (bottom), showing the transmitters and receivers for each operation.

8 Results and Discussion

The results presented in this section build on the experimental and simulation work carried out during the internship. Laboratory investigations using commercial OOK transceivers provided insight into the relationship between input optical power, SNR, and receiver sensitivity under both direct-detection and coherent reception schemes. These measurements established benchmarks for the minimum optical power required to achieve reliable signal recovery at the PD output. Parallel efforts focused on developing a Python-based simulation tool to model PICs, enabling quantitative assessment of power loss, noise contributions, and SNR across different architectures. The outcomes of these experiments and simulations are discussed in the following subsections, with attention to how they inform the design and evaluation of multi-function PIC transceivers for high-throughput optical communication applications.

8.1 Lab Experiments

To complement the modeling work, laboratory experiments were conducted to characterize the performance of COTS OOK transceivers under varying operating conditions. These experiments focused on measuring the relationship between input optical power, noise power, and SNR at the PD output, both for direct-detection and coherent reception schemes. By adjusting parameters such as gain, attenuation, and LO power, the experiments provided practical benchmarks for transceiver sensitivity and highlighted the trade-offs between detection methods, amplifier use, and system noise contributions.

8.1.1 IM-DD Sensitivity

The aim of this experiment was to examine the effect of input optical power on the electrical power, noise power, and SNR of an OOK transceiver under intensity-modulation direct-detection (IM-DD), in order to determine its sensitivity. The input power at the PD was varied using a VOA for a range of (3 - -55) dBm, which encompasses the range of values expected for the power of the signal at the receiver for inter-satellite links.
The measured performance of the IM-DD system is summarized in terms of noise, signal level, and resulting SNR as functions of input power. The signal voltage was obtained by measuring the peak-to-peak value for an average of 2000 counts on the oscilloscope. The noise voltage was obtained by measuring the variance about a perfectly horizontal line in an expected, noiseless signal. The SNR for electronics was then computed from the formula in Eq. (6).

$$\mathrm{SNR}_{\mathrm{dB}} = 20 \cdot \log_{10}\left(\frac{\text{signal}}{\text{noise}}\right) \tag{6}$$

Fig. 20 shows the relationship between the signal and input power, with a TIA in the loop and without a TIA. The TIA plot increases exponentially until approximately 0 dBm where it begins to flatten, revealing a tendency towards saturation which suggests a limit in the effective optimal range for TIA operation. Fig 21 shows the relationship between the noise and input power. The plot shows a relatively flat noise floor until approximately -5 dBm, where input-dependent contributions such as RIN or shot noise dominate. An exponential curve was fitted onto the data to show the observed trend on a logarithmic-linear scale. If both scales were linear, the fitted curve will most likely be a line, showing a linear trend between SNR and input power.
These plots show that by increasing the input power, an increase in both signal and noise is observed. From the exponential equations of the fitted lines, the growth constants of the no TIA data for the signal and the noise are 0.353 and 0.299, showing that as the input

power decreases, the signal will decay quicker than the noise. For the TIA plots, the growth constants for the signal and the noise were 0.164 and 0.147, showing that by introducing a TIA in the loop, the decrease in signal and noise with decreasing input power is less than with no TIA after the PD. The difference between the growth constants is also smaller in the TIA plots than the no TIA plots, showing that a TIA in the circuit minimises the difference between the decreases in signal and noise with decreasing input power. The voltages for both signal and noise plots never reach 0 mV showing there is a noise floor present, likely due to dark current and thermal noise.

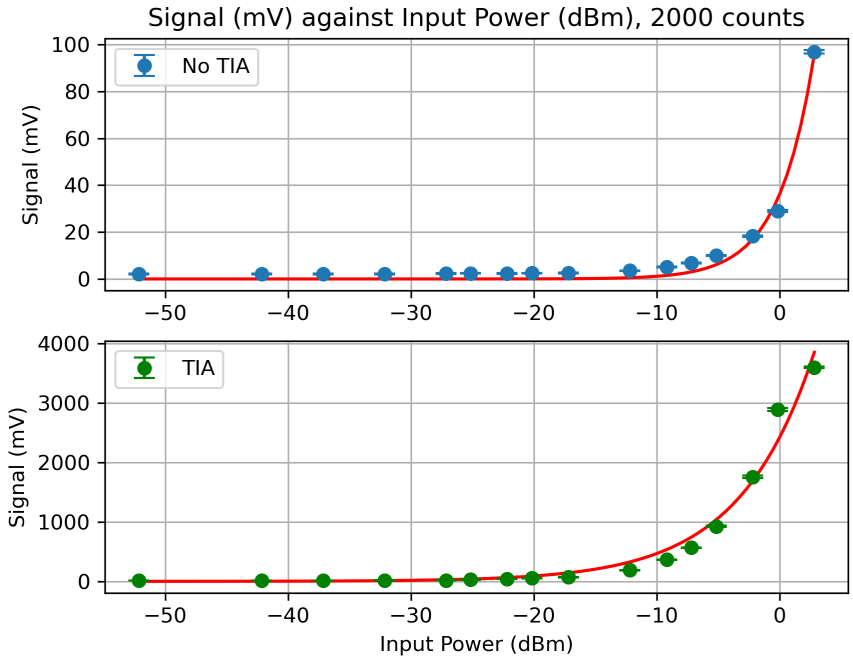


Figure 20: Signal against Input power for the OOK transceiver using IM-DD reception.

The SNR against input power plot shown in Fig. 22 highlights the combined effects of the signal and noise plots. This is shown through the exponential growth plot obtained, showing similarity to the signal and noise trends. The SNR improves exponentially as the input power increases, indicating enhanced symbol detectability and reduced bit error probability at higher input powers. This exponential behaviour is not seen in the TIA plot, however. After approximately -10 dBm, the curve flattens and the SNR no longer increases with input power. This can be explained from the TIA operation where after a certain input power, the TIA runs out of headroom and the effective transimpedance shrinks, clipping the signal. The noise continues to increase, however, as shot noise increases with photocurrent. This is also seen in the noise against input power plot in Fig. 21, where at higher powers, the noise signal is dominated by shot noise. Though the TIA adds noise to the system, it improves the signal link. For example, the plot shows that the input power required for a minimum of 10 dB SNR is approximately -10 dBm input power, but this minimum input power decreases to -20 dBm when a TIA is introduced into the system. This means that a TIA allows a lower input power to still achieve a decodable SNR value than systems without a TIA, showing why FSO systems use TIAs despite the additional noise.

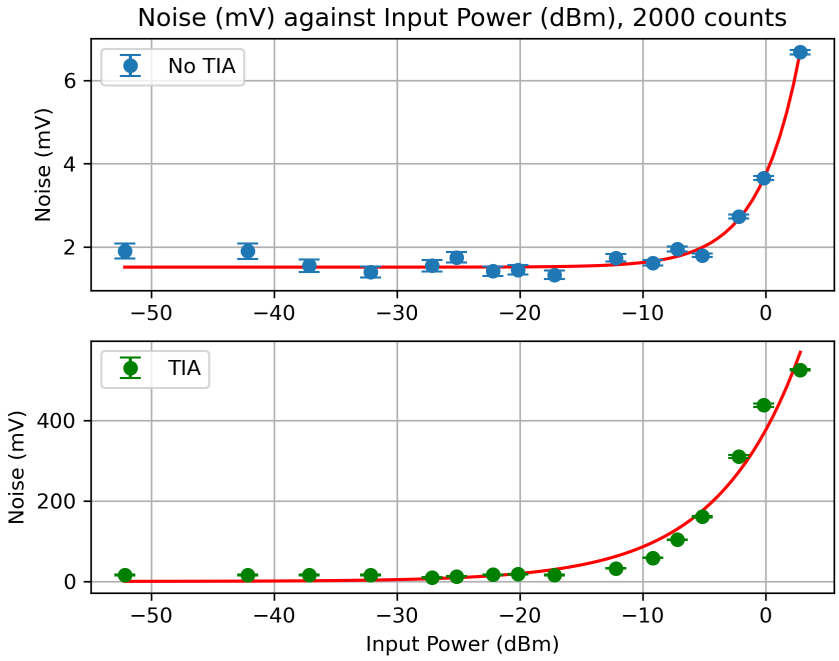


Figure 21: Noise against Input power for the OOK transceiver using IM-DD reception.

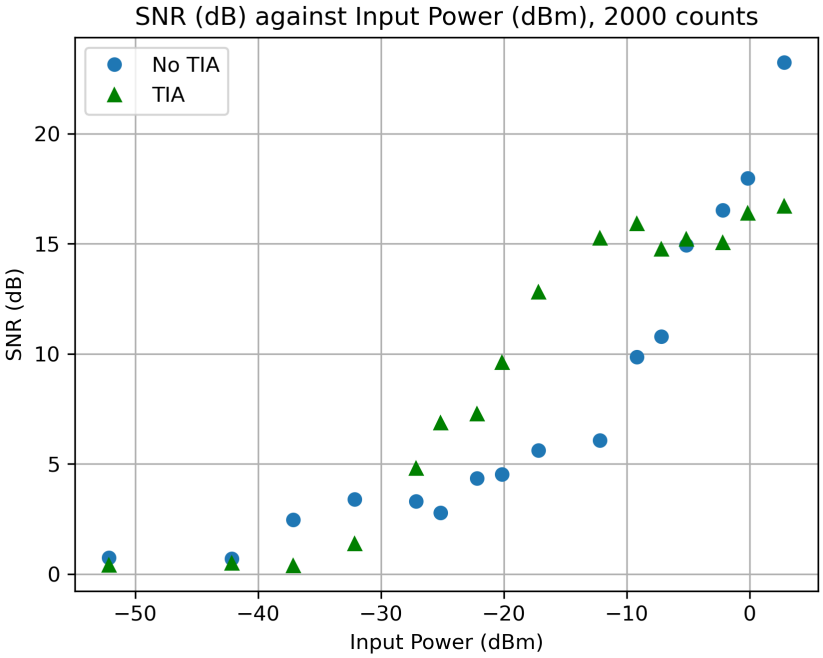


Figure 22: SNR against Input power for the OOK transceiver using IM-DD reception.

8.1.2 Coherent Sensitivity

The aim of this experiment was to evaluate the performance of the OOK transceiver using a coherent receiver and to compare the resulting SNR and sensitivity with those obtained under direct detection. The coherent detection measurements were analyzed using three different plots: received signal power as a function of VOA voltage, SNR gain as a function of amplifier gain, and SNR as a function of input optical power. The setup was kept similar as before, with the transceiver connecting to the coherent receiver board that connected to a PD then finally to the TIA. An LO at a constant 8 dBm power was mixed with the signal before being detected by the PD. The SNR was obtained in the same way as for the direct detection method.
The SNR against input power in Fig. 23 follows a similar trend as the direct detection method, where the SNR improves as the input power increases. Since there is a TIA in the loop, it is expected to see a saturation at some input power as in the direct detection method which is not seen in the coherent detection. This may mean that saturation occurs at higher input power which could be due to a difference in the TIA model that is in the coherent receiver. The SNR values are roughly similar to that of direct detection. The expected trend is that the coherent reception method should have a better performance than the direct detection method, because the LO gain amplifies the signal beyond the noise floor for a shot-noise limited operation (Yamakawa, Araki, and Hisada 1999; Zahr et al. 2024). A reason for the similar SNR values is that the LO is contributing its own noise, like RIN and phase noise, which is being picked up by the coherent receiver since it is sensitive to phase and polarisation information, unlike direct detection which is only intensity sensitive.

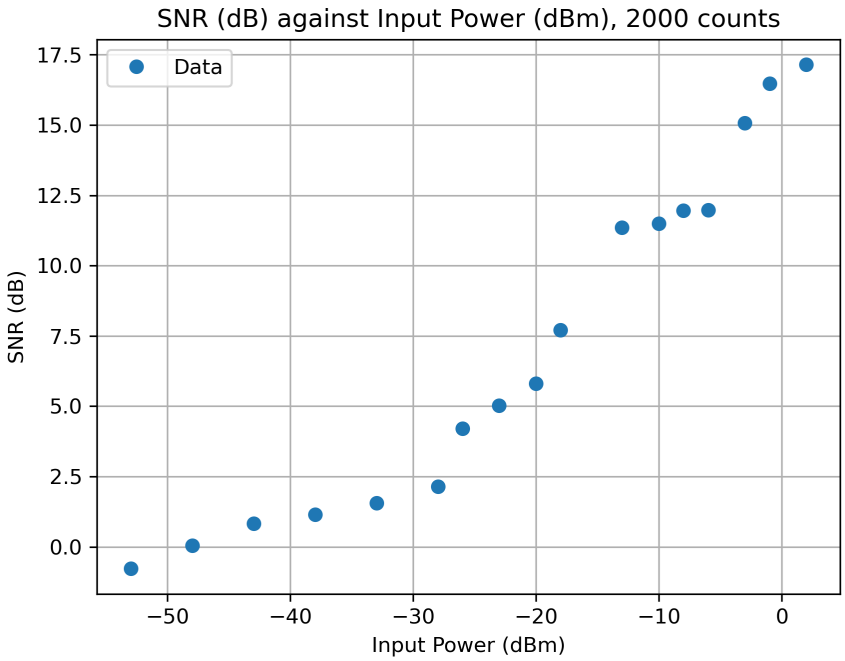


Figure 23: SNR against Input power for the OOK transceiver using coherent reception.

To ensure the SNR results obtained were optimised, receiver board parameters were swept through a range of values to ensure the highest performance when taking the SNR values. The receiver board GUI allowed the internal VOA and TIA gain to be varied.
The coherent receiver datasheet stated the VOA can attenuate up to 10 dB within a voltage

range of (0 - 5) V. An investigation was conducted to assess the relation between the VOA voltage and the attenuation. The VOA voltage was swept through a range of (0 - 5) V while the input power was kept constant. The plot in Fig. 24 shows that the relationship is not linear, but follows a more parabolic curve as the VOA voltage increases. This non-linear behaviour was also prevalent in the external VOA used in to vary the optical input power, where the attenuation increased exponentially with voltage. The plot shows the signal power increasing with VOA voltage, which is different from the external VOA since this means the attenuation decreases with increasing voltage. The peak signal power was reached when the VOA voltage was at approximately 3.5 V, so this was the VOA value applied when taking SNR measurements. Past this point, the signal shows a decrease as the attenuation decreases; the expected behaviour is that the signal power should increase with a decrease in VOA attenuation. An explanation for this behaviour is that more current is inputted than the VOA can take so it no longer changes the attenuation. The datasheets give info about the optimal voltage range, attenuation range and current range, without any information on the electrical resistance to see how well the voltage and current ranges correlate. Another explanation is that the raw optical power may actually be increasing, but the integrated TIA saturates and clips the photocurrent signal, reducing the signal metric. This behaviour is also shown in the direct detection method, where after a sufficient enough input power, the TIA is no longer in its optimal operation range and begins to compress the signal.

The TIA gain is another parameter of the coherent receiver that was varied. The gain can be optimised by a control voltage, which was swept through a range of (0.1 - 1.7) V while maintaining a constant input power. The plot shown in, Fig. 25, shows an overall trend of a decrease in SNR as the gain increases. A 'jump' in SNR is seen between 0.6 and 1.1 dB gain. This behavior may indicate that the integrated TIA has an optimal operating window around 0.6–0.8 dB gain, where the signal is strong enough to overcome quantization noise but not yet limited by excess TIA/ADC noise or bandwidth loss. Increasing gain beyond ~1.0 leads to diminishing returns and eventually a collapse in SNR, caused by a combination of excess amplifier noise and reduced linear bandwidth. Thus, the TIA gain value chosen to obtain the SNR results was 0.7 dB.

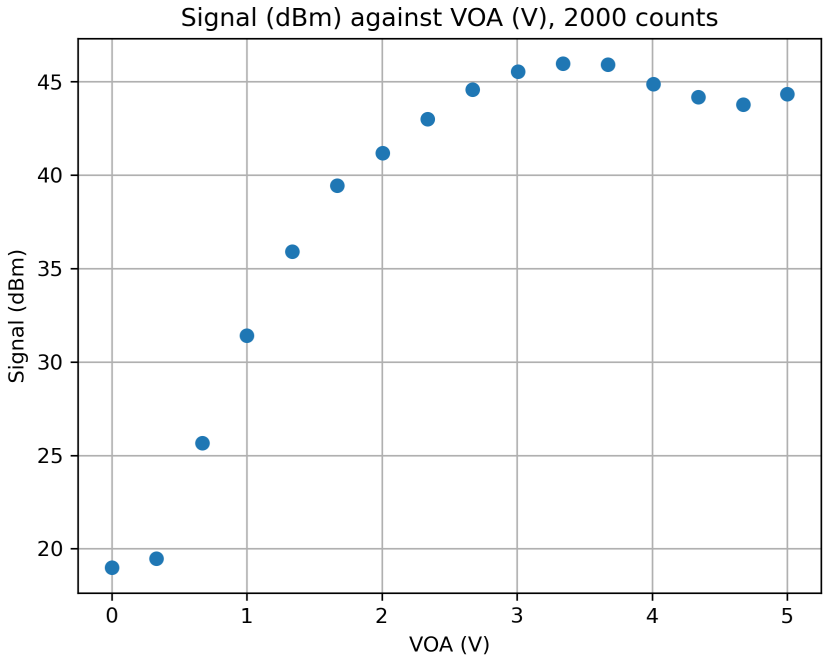


Figure 24: Signal against receiver board VOA attenuation for the OOK transceiver using coherent reception.

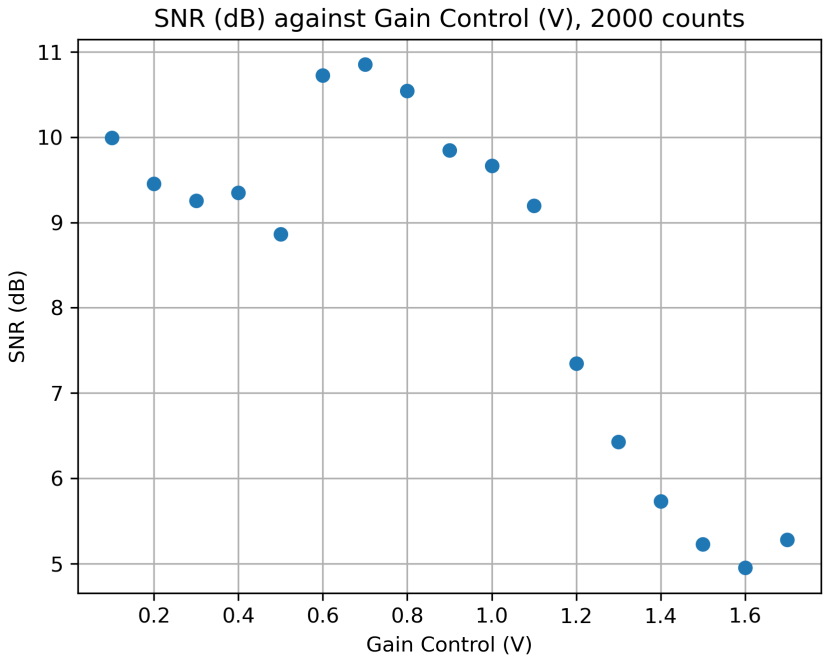


Figure 25: SNR against receiver board Gain Control Voltage for the OOK transceiver using coherent reception.

8.1.3 LO Impact

The aim of this experiment was to investigate the influence of local oscillator (LO) power on coherent receiver performance, with the goal of identifying the optimum LO operating point that maximizes SNR while accounting for additional noise sources.
As of writing this report, this work has not been fully completed yet. The plan is to use the same setup as in the coherent reception experiment. Then, the LO power will be swept through a range of (0 - 20) dBm while the input power and receiver board parameters are kept constant. The SNR will be obtained by a similar method as in the coherent reception and plot of SNR against LO input power will be created to assess a trend.

8.2 Simulation Software

The aim of this task was to develop a simulation environment capable of modeling photonic integrated circuits and transceivers, in order to analyze power loss, noise contributions, and SNR across different architectures prior to fabrication.
As of writing this report, this work has not been fully completed yet. The base Simphony library has the S-parameter simulation function along with some common photonic components already implemented. However, important components that would be used in the design of the multi-function transceiver, such as MZMs, do not exist in base Simphony. The library offers a simple method for creating components given that the component's effect on the input complex value is known. The components that have been added are erbium-doped fiber amplifiers (EDFAs), which are not PIC components, though they are used in the complete transceiver system after transmitting and before reception through the free-space channel. A constant power EDFA, which outputs a constant power given that the input power is above a set threshold, is connected to the output of a PIC before it is launched into the free-space channel to mitigate the losses the atmosphere will incur on the signal. A constant gain EDFA, which amplifies the input signal by a constant dB gain given that it is above a set threshold, is usually placed after the free-space channel to boost the signal for optimal operation in the receiver PIC.
Figs. 26 and 27 show the expected logic flow of the simulation tool when complete. Python files containing useful functions were created and imported into main, where the circuit and parameters are inputted and requested KPI are outputted. The PICcircuits file contains the circuit instances, models, parameters, and ports, which are parsed into a circuit operator class defined in PICfunctions. This operator class can manipulate the circuit, such as defining a subcircuit between the whole circuit, and perform simulations on it. The PICfunctions file also contains a component operator class, which parses in components and their parameters as given from foundries and creates custom models for simulation. The PICcomponents file will house additional components made, such as EDFAs, while the PICcomponents_SNR file will house the noise sources of the models defined in PICcircuits to perform calculations such as SNR and KPI grading.
The current flow of simulating a circuit with the simulation tool is as follows:

- Parameters are written into a .csv spreadsheet,
- Circuits are created in a .csv spreadsheet in order of appearance (input to output),
- The Simphony Simulator code parses the data from the spreadsheets and applies it to the components to create a 'netlist' for simulation,
- A snapshot is output containing information such as the circuit that was simulated and the scored KPI to give a relative idea on the circuits performance.

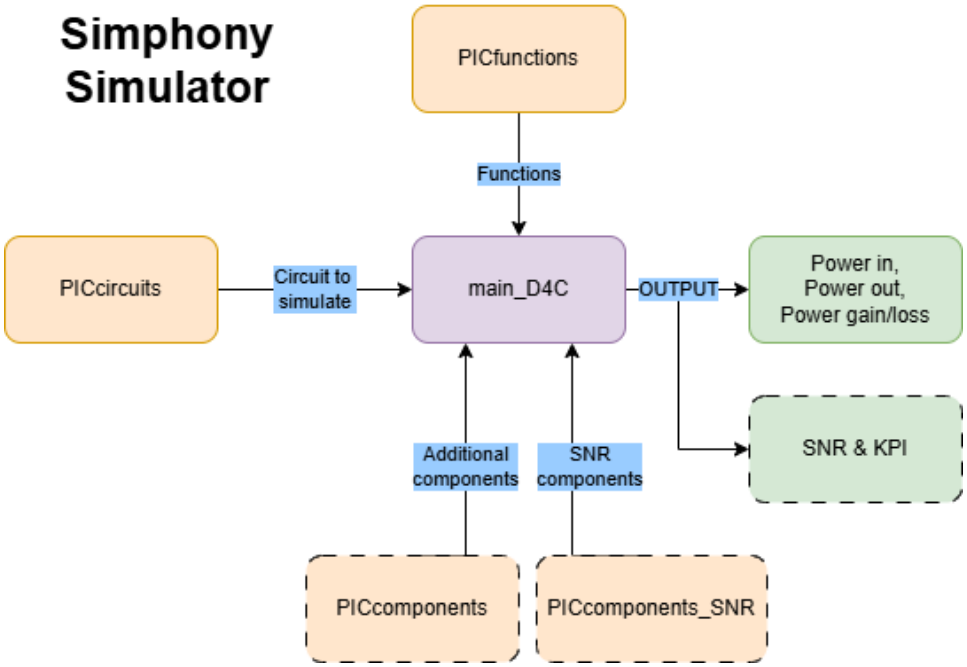


Figure 26: Block diagram of the simphony simulator software logic. Full boxes indicate they are implemented, dashed boxes indicate they are not yet implemented, but planned. Purple boxes indicate 'main'; Orange boxes indicate inputs; Green boxes indicate outputs.

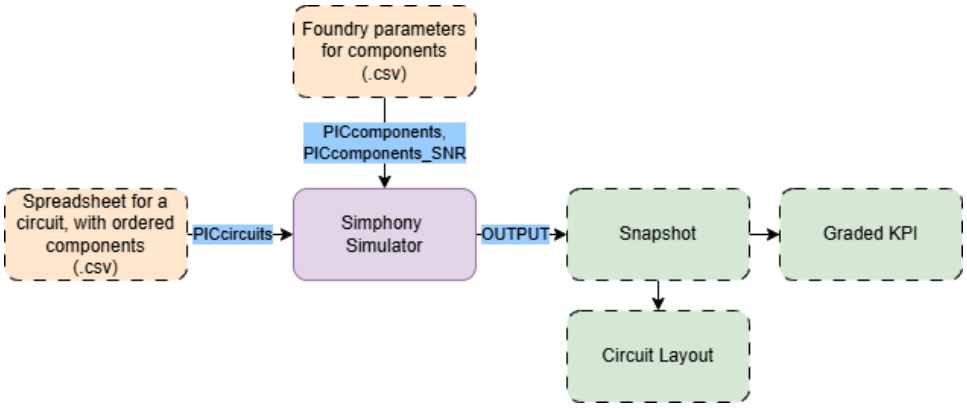


Figure 27: Block diagram of the simulation software tool logic. Full boxes indicate they are implemented, dashed boxes indicate they are not yet implemented, but planned. Purple boxes indicate 'main'; Orange boxes indicate inputs; Green boxes indicate outputs.

8.3 Photonic System Architecture

The aim of this study was to investigate candidate architectures for a multi-function photonic transceiver supporting OOK and PM-QPSK modulation, with the objective of identifying designs that balance data rate, SNR, bandwidth, and SWaP requirements.
As of writing this report, this work has not yet been completed. Fig. 28 shows a sample scenario of OOK operation for a satellite feeder link. This circuit gives the expected link budget for linking to a satellite at 50 degrees in LEO. This system, along with the OOK circuit shown in Fig. 19, have been reconstructed inside of the Simphony simulator to assess the power gain/loss. With a transmitter laser power of 1 mW, the optical power at the PD in the receiver gave 0.015 mW, or -18.2 dBm. If the transceiver used was that from the lab experiments, using Fig. 22 gives an SNR of 5 dB for no TIA, and an SNR of approximately 10 dB with a TIA. This is a reasonable value within the expected range, showing a promising outlook for the simulation tool's effectiveness and accuracy. The 'main' code that was run can be found in the appendix 1.

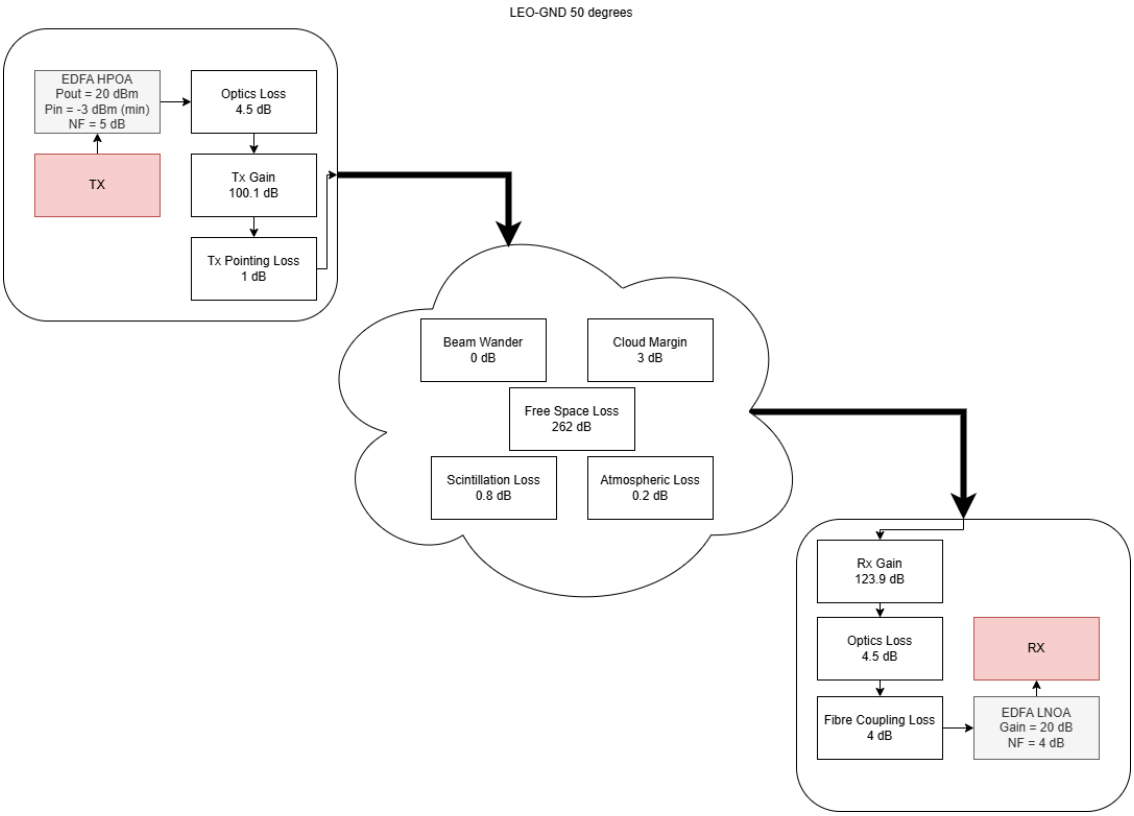


Figure 28: Example scenario of a feeder link to a satellite in LEO orbit at 50 degrees, showing the expected link budget for an OOK operation.

9 Conclusion

This work combined experimental measurements with preliminary simulation efforts to assess the performance of COTS OOK transceivers under direct detection and coherent reception, as well as to begin the development of a photonic circuit simulation tool. Coherent receivers can be used in both coherent reception and direct detection, while direct detection methods are insensitive to phase, and thus, coherent reception. A comparison to understand the operations of both methods for an OOK operation motivated the experimental work. Laboratory results demonstrated the relationship between input optical power, signal strength, noise contributions, and resulting SNR, establishing sensitivity benchmarks for commercial OOK transceivers. Direct-detection measurements showed an exponential dependence of SNR on input power, with the TIA introducing both performance improvements at low powers and saturation effects at higher powers. However, for the same SNR, the system with a TIA allowed a lower input power than the system without a TIA, -20 dBm and -10dBm for an SNR of 10 dB respectively. Coherent reception experiments revealed broadly similar SNR values to direct detection, with analysis highlighting the competing influences of LO gain and LO noise, as well as the importance of optimal VOA and TIA settings to maximize performance.
A Python-based simulation environment began development which provided the foundation for modeling photonic integrated circuits, with initial implementations of amplifier components and circuit handling functions. Although not yet complete, this tool shows potential for enabling quantitative assessment of system-level performance metrics such as SNR and insertion loss before fabrication. For example, the tool was used to simulate a feeder link to a LEO satellite at 50 degrees using OOK operation resulting in an SNR of 10 dB and 5 dB if using the COTS transceiver with and without a TIA respectively.
Overall, the results highlight the critical role of receiver front-end design in determining transceiver sensitivity, the operational trade-offs between direct-detection and coherent schemes, and the importance of accurate simulation frameworks for guiding architecture choices. Future work will extend the coherent receiver characterization to include systematic LO power sweeps, expand the component library of the simulation tool, and apply the framework to evaluate candidate multi-function PIC transceiver architectures for high-throughput optical satellite communication links.

References

AscentOptics (2024). "Fiber Optic Cables: Advantages, Disadvantages, and Use Cases". In: *AscentOptics Blog*.

Barrueco, Jon et al. (2021). "Constellation Design for Future Communication Systems: A Comprehensive Survey". In: *IEEE Access* 9, pp. 89778–89797. doi: 10.1109/ACCESS.2021.3090774.

Boroson, Don M. et al. (Mar. 2014). "Overview and results of the Lunar Laser Communication Demonstration". In: *Free-Space Laser Communication and Atmospheric Propagation XXVI*. Ed. by Hamid Hemmati and Don M. Boroson. Vol. 8971. SPIE, 89710S. doi: 10.1117/12.2045508.

Burr, Phil (2024). "How optical interconnect and optical processing are changing data centers". In: *The Compute, Storage Networking Channel*.

Camuñas-Mesa, Luis and José Rosa (Nov. 2023). "Combining Software-Defined Radio Learning Modules and Neural Networks for Teaching Communication Systems Courses". In: *Information* 14, p. 599. doi: 10.3390/info14110599.

Cheng, Yongpeng et al. (2014). "InGaAs MSM photodetector monolithically integrated with InP photonic-wire waveguide on III-V CMOS photonics platform". In: *IEICE Electronics Express* 11.16, pp. 20140609–20140609. issn: 1349-2543. doi: 10.1587/elex.11.20140609.

Clark, S. (2021). "SpaceX launches first full batch of laser-equipped Starlink satellites". In: *Spaceflight Now*. url: https://spaceflightnow.com/2021/09/14/spacex-launches-first-full-batch-of-laser-equipped-starlink-satellites/.

Conroy, Philip et al. (June 2018). "Demonstration of 40GBaud intradyne transmission through worst-case atmospheric turbulence conditions for geostationary satellite uplink". In: *Applied Optics* 57.18, p. 5095. issn: 2155-3165. doi: 10.1364/ao.57.005095.

Dhumal, Amol R., Atul P. Kulkarni, and Nitin H. Ambhore (Nov. 2023). "A comprehensive review on thermal management of electronic devices". In: *Journal of Engineering and Applied Science* 70.1. issn: 2536-9512. doi: 10.1186/s44147-023-00309-2.

Doerr, C. R. (2010). "Photonic Integrated Circuits for High-Speed Communications". In: *Conference on Lasers and Electro-Optics 2010*. Optica Publishing Group, CFE3. doi: 10.1364/CLEO.2010.CFE3. url: https://opg.optica.org/abstract.cfm?URI=CLEO-2010-CFE3.

EffectPhotonics (May 2023). "The Fabrication Process Inside a Photonic Foundry". In: *Insights*. url: https://effectphotonics.com/insights/the-fabrication-process-inside-a-photonic-foundry/.

Eguri, Samson Vineeth Kumar, Arockia Bazil Raj A, and Nishant Sharma (July 2022). "Survey on acquisition, tracking and pointing (ATP) systems and beam profile correction techniques in FSO communication systems". In: *Journal of Optical Communications* 45.4, pp. 881–904. issn: 2191-6322. doi: 10.1515/joc-2021-0222.

Eldada, Louay (Mar. 2004). "Optical communication components". In: *Review of Scientific Instruments* 75.3, pp. 575–593. issn: 1089-7623. doi: 10.1063/1.1647701.

Farjadrad, Ramin (2014). "What's the Difference Between Optical and Electrical Technology for 100-Gbit/s Connectivity in Future Systems?" In: *ElectronicDesign Communications*.

Fuchs, Christian and Christopher Schmidt (July 2019). "Update on DLR's OSIRIS program". In: *International Conference on Space Optics — ICSO 2018*. Ed. by Nikos Karafolas, Zoran Sodnik, and Bruno Cugny. SPIE, p. 17. doi: 10.1117/12.2535937.

Al-Gailani, Samir Ahmed et al. (2021). "A Survey of Free Space Optics (FSO) Communication Systems, Links, and Networks". In: *IEEE Access* 9, pp. 7353–7373. issn: 2169-3536. doi: 10.1109/access.2020.3048049.

Goswami, Arnab et al. (2024). "Material platforms for integrated photonics". In: *On-Chip Photonics*. Elsevier, pp. 91–131. isbn: 9780323917650. doi: 10.1016/b978-0-323-91765-0.00014-1.

Heine, Frank et al. (2014). "The European Data Relay System, high speed laser based data links". In: *2014 7th Advanced Satellite Multimedia Systems Conference and the 13th Signal Processing for Space Communications Workshop (ASMS/SPSC)*, pp. 284–286. doi: 10.1109/ASMS-SPSC.2014.6934556.

Iwai, Hiroshi and Shun'ichiro Ohmi (Apr. 2002). "Silicon integrated circuit technology from past to future". In: *Microelectronics Reliability* 42.4–5, pp. 465–491. issn: 0026-2714. doi: 10.1016/s0026-2714(02)00032-x.

JAXA, ESA - and their respective Industries (July 2024). *ESA SPECIFICATION FOR TERABIT/SEC OPTICAL LINKS (ESTOL)*.

K., K. Ghosh (Mar. 2011). "Noise in Electronic and Photonic Devices". In: *Advances in Photodiodes*. InTech. isbn: 9789533071633. doi: 10.5772/15223.

Kikuchi, Kazuro (Jan. 2016). "Fundamentals of Coherent Optical Fiber Communications". In: *Journal of Lightwave Technology* 34.1, pp. 157–179. issn: 1558-2213. doi: 10.1109/jlt.2015.2463719.

Klamkin, Jonathan et al. (Oct. 2018). "Indium Phosphide Photonic Integrated Circuits: Technology and Applications". In: *2018 IEEE BiCMOS and Compound Semiconductor Integrated Circuits and Technology Symposium (BCICTS)*. IEEE, pp. 8–13. doi: 10.1109/bcicts.2018.8550947.

Komljenovic, Tin et al. (July 2017). "Widely-Tunable Ring-Resonator Semiconductor Lasers". In: *Applied Sciences* 7.7, p. 732. issn: 2076-3417. doi: 10.3390/app7070732.

Kumar, Lokesh, Naveed Saqib, and Imdad Hussain (2024). "Emerging Trends in Free Space Optical Communication: Photonics Integrated Circuits and Lithium Niobate Technologies". In.

Lucovsky, G., R. F. Schwarz, and R. B. Emmons (Mar. 1964). "Transit-Time Considerations in p—i—n Diodes". In: *Journal of Applied Physics* 35.3, pp. 622–628. issn: 1089-7550. doi: 10.1063/1.1713426.

Mata Calvo, Ramon et al. (Mar. 2019). "Optical technologies for very high throughput satellite communications". In: *Free-Space Laser Communications XXXI*. Ed. by Hamid Hemmati and Don M. Boroson. SPIE, p. 31. doi: 10.1117/12.2513819.

Miyamoto, Yutaka and Hirokazu Takenouchi (Dec. 2014). "Dense Space-division-multiplexing Optical Communications Technology for Petabit-per-second Class Transmission". In: *NTT Technical Review* 12.12, pp. 43–49. issn: 2436-5327. doi: 10.53829/ntr201412ra3.

Mukherjee, Biswanath et al. (2020). *Springer handbook of optical networks*. Springer Nature.

Ogiso, Yoshihiro et al. (Apr. 2017). "Over 67 GHz Bandwidth and 1.5 V Vπ InP-Based Optical IQ Modulator With n-i-p-n Heterostructure". In: *J. Lightwave Technol.* 35.8, pp. 1450–1455. url: https://opg.optica.org/jlt/abstract.cfm?URI=jlt-35-8-1450.

Paschotta, R. (2008). "Semiconductor Optical Amplifiers - an encyclopedia article". In: *RP Photonics Encyclopedia*. RP Photonics AG. doi: 10.61835/2he.

Ploeg, Sequoia, Hyrum Gunther, and Ryan M. Camacho (2021). "Simphony: An Open-Source Photonic Integrated Circuit Simulation Framework". In: *Computing in Science & Engineering* 23.1, pp. 65–74. doi: 10.1109/MCSE.2020.3012099.

Raj, Arockia Bazil and Arun K. Majumder (Oct. 2019). "Historical perspective of free space optical communications: from the early dates to today's developments". In: *IET Communications* 13.16, pp. 2405–2419. issn: 1751-8636. doi: 10.1049/iet-com.2019.0051.

Sabol, Dusan et al. (Dec. 2008). "Investigation of Some Issues of Full Optical Multimedia Networks". In: *Komunikacie* 10, pp. 58–63. doi: 10.26552/com.C.2008.4.58-63.

Saracco, Roberto (Apr. 2019). "Rivers of bits under the oceans". In: *IEEE Future Directions*.

Selvaraja, Shankar Kumar and Purnima Sethi (Aug. 2018). "Review on Optical Waveguides". In: *Emerging Waveguide Technology*. InTech. isbn: 9781789234930. doi: 10.5772/intechopen.77150.

Smit, Meint, Kevin Williams, and Jos van der Tol (May 2019). "Past, present, and future of InP-based photonic integration". In: *APL Photonics* 4.5. issn: 2378-0967. doi: 10.1063/1.5087862.

Sree Madhuri, A., Govardhani Immadi, and M. Venkata Narayana (Mar. 2020). "Estimation of Effect of Fog on Terrestrial Free Space Optical Communication Link". In: *Wireless Personal Communications* 112.2, pp. 1229–1241. issn: 1572-834X. doi: 10.1007/s11277-020-07098-4.

Staelin, David (2009). "Electromagnetics and Applications". In: *MIT OpenCourseWare*.

Steinhauer, Stephan, Samuel Gyger, and Val Zwiller (Mar. 2021). "Progress on large-scale superconducting nanowire single-photon detectors". In: *Applied Physics Letters* 118.10. issn: 1077-3118. doi: 10.1063/5.0044057.

Surof, Janis, Juraj Poliak, and Ramon Mata Calvo (June 2017). "Demonstration of intradyne BPSK optical free-space transmission in representative atmospheric turbulence conditions for geostationary uplink channel". In: *Opt. Lett.* 42.11, pp. 2173–2176. doi: 10.1364/OL.42.002173. url: https://opg.optica.org/ol/abstract.cfm?URI=ol-42-11-2173.

Taubenblatt, Marc A. (2012). "Optical Interconnects for High-Performance Computing". In: *Journal of Lightwave Technology* 30.4, pp. 448–457. doi: 10.1109/JLT.2011.2172989.

Terrasanta, Giulio, Marcin Wojciech Ziarko, et al. (Jan. 2025). "Photonic Integrated Circuits for Optical Satellite Links: A Review of the Technology Status and Space Effects". In: *International Journal of Satellite Communications and Networking* 43.3, pp. 210–228. issn: 1542-0981. doi: 10.1002/sat.1552.

Terrasanta, Giulio, Agnes M. Zinth, et al. (Apr. 2025). "Total Ionizing Dose Effects on Silicon Nitride Photonic Integrated Microring Resonators and Mach–Zehnder Interferometers". In: *IEEE Transactions on Nuclear Science* 72.4, pp. 1542–1551. issn: 1558-1578. doi: 10.1109/tns.2025.3550647.

Toyoshima, Morio (June 2005). "Trends in satellite communications and the role of optical free-spacecommunications (Invited)". In: *J. Opt. Netw.* 4.6, pp. 300–311. doi: 10.1364/JON.4.000300. url: https://opg.optica.org/jon/abstract.cfm?URI=jon-4-6-300.

Vyshnevyy, Andrey A. et al. (Aug. 2023). "van der Waals Materials for Overcoming Fundamental Limitations in Photonic Integrated Circuitry". In: *Nano Letters* 23.17, pp. 8057–8064. issn: 1530-6992. doi: 10.1021/acs.nanolett.3c02051.

Yamakawa, Shiro, Tomohiro Araki, and Yasumasa Hisada (Apr. 1999). "<title>Trade-off between IM-DD and coherent system in high-data-rate optical interorbit links</title>". In: *Free-Space Laser Communication Technologies XI*. Ed. by G. Stephen Mecherle. Vol. 3615. SPIE, pp. 80–89. doi: 10.1117/12.346205.

Zahr, Ayman et al. (2024). "An Information-Theoretic Comparison Between Coherent and IM/DD Transmissions for Free Space Optical Communications". In: *IEEE Journal on Selected Areas in Communications* 42.5, pp. 1304–1315. doi: 10.1109/JSAC.2024.3365898.

Zhao, Zheng et al. (Oct. 2017). "Optical computing on silicon-on-insulator-based photonic integrated circuits". In: *2017 IEEE 12th International Conference on ASIC (ASICON)*. IEEE, pp. 472–475. doi: 10.1109/asicon.2017.8252516.

Zhu, Xiaotian et al. (Mar. 2023). "Low-loss fiber-to-chip edge coupler for silicon nitride integrated circuits". In: *Optics Express* 31.6, p. 10525. issn: 1094-4087. doi: 10.1364/oe.483907.

Ziarko, Marcin et al. (Mar. 2024). "Photonic integrated circuits for high-throughput optical communications and ranging satellite links". In: *Free-Space Laser Communications XXXVI*. Ed. by Hamid Hemmati and Bryan S. Robinson. SPIE, p. 15. doi: 10.1117/12.3001792.

10 Appendix

```

from PICcircuits import *
from PICfunctions import calculate_edfapower_in, CircuitOperator

path = 'components/FraunhoferHHIv1.xlsx'
sim_circuit = get_circuit('ook', path) # Define circuit to simulate
power_in = 1 # mW

circuit = CircuitOperator(sim_circuit) # Create circuit operator

edfa_powerin = calculate_edfapower_in(circuit, power_in=power_in) #
    Calculates power at edfa input for constant power output calculation

circuit.update({  # Updating the circuit component parameters
    "wg_input": {"length": 1000.0, "pos": "shallow", "pol": "te"},
    "edfa_power" : {'power_out': 20, 'power_in': edfa_powerin}, #dBm, mW
    "postchannel": {'gain': 135.4},  # dB
    "wg_output": {"length": 1000.0, "pos": "deep", "pol": "tm"},
})

# Simulation
circuit.result(result='power')
```

Listing 1: Example main code used to simulate the OOK operation satellite feeder link scenario.